Designing Biosensors to Detect the Activity of Signaling Pathways during Host-Microbe Interactions

by

Genevieve Marie Weist

Bachelor of Science, University of Delaware, 2016

Submitted to the Graduate Faculty of

The Kenneth Dietrich School of Arts and Sciences in partial fulfillment

of the requirements for the degree of

Master of Science

University of Pittsburgh

2019

UNIVERSITY OF PITTSBURGH

DIETRICH SCHOOL OF ARTS AND SCIENCES

This thesis was presented

by

Genevieve Marie Weist

It was defended on

November 9, 2018

and approved by

Stephen Weber, Professor, Department of Chemistry

Alexander Deiters, Professor, Department of Chemistry

Thesis Advisor/Dissertation Director: W. Seth Childers, Assistant Professor, Department of Chemistry

Copyright © by Genevieve Marie Weist

2019

Designing Biosensors to Detect the Activity of Signaling Pathways during Host-Microbe Interactions

Genevieve Marie Weist, MS

University of Pittsburgh, 2019

During chronic infections, pathogenic microbes colonize host environments by forming biofilms, a process that is orchestrated by signaling systems. These signaling systems, sensitive to both host and co-habitating bacteria, help to recruit individual microbes to the biofilm, selectively target and kill invasive microbes, and promote biofilm dispersal.[1] Formation of bacterial biofilms in cystic fibrosis patients by *Pseudomonas aeruginosa* microbes triggers the transition from acute to chronic infection in compromised airways. Unfortunately, due to lack of direct methods to detect signaling activity in living cells, signals within signaling systems have been difficult to identify in *P. aeruginosa*. We propose the development of strategies to track the activity of bacterial signaling proteins to elucidate mechanisms of host-microbe interactions.

We aim to develop tools to determine the signals utilized in biofilm formation, visibly and instantaneously. To do so, we utilize dimerization dependent green fluorescent proteins (ddGFPs),[2] circular permuted green fluorescent protein (cpGFP),[3] and a fluorescent protein gene reporter as outputs of the two-component signaling system from *P. aeruginosa.* These biosensors will allow us to track the

downstream activation of signaling systems and the corresponding biofilm formation in living cells.

Table of Contents

List of Figures

Introduction

Pseudomonas aeruginosa biofilm forms in response to different signals

Pseudomonas aeruginosa is a gram-negative pathogenic bacterium known to survive in soil and water environments, including inside the other residents of these environments: plants, insects, and animals. Among humans, *P. aeruginosa* is a major concern for hospitals, as it's the third most common hospital pathogen. An infection of *P. aeruginosa* in an immunocompromised patient commonly results in death.[4] This is due to the adaptive and mutational responses of *P. aeruginosa.* With the rise of antibiotics, acute infections were able to be treated. The over-prescription of antibiotics to treat a chronic *P. aeruginosa* infections has in part led to multi-drug resistant strains.[5] The factors that cause chronic infections to be untreatable is *P. aeruginosa*'s innate adaptability and resistance mechanisms.[5] The adaptability mechanisms which allow the bacterium to infiltrate various environments relies on communication networks between the bacteria, called quorum sensing (QS).[1] These signaling networks interpret the extracellular environment and respond with changes in resistance mechanisms gene expression.

The transition from acute bacterial infections to chronic infections involves the formation of biofilms. Biofilm development requires the initial attachment of bacteria to a surface, followed by the formation of microcolonies and the production of a polymeric matrix surrounding the biofilm.[6] The matrix is made of polysaccharides, DNA, proteins, and small molecules.[6] This protected system allows

for the cells to upregulate virulence genes to resist against antimicrobial agents and host defense systems. Various signals, such as divalent metals, cell death debris, host-secreted antimicrobial peptides, small molecules, and pH, report to the *P. aeruginosa* cells about the surrounding kin and host cells. These allow the *P. aeruginosa* to initiate a group response. Environmental signals change at each stage of biofilm formation based on the needs of the bacteria such as safety from the host, or a need for more nutrients. (Figure 1)

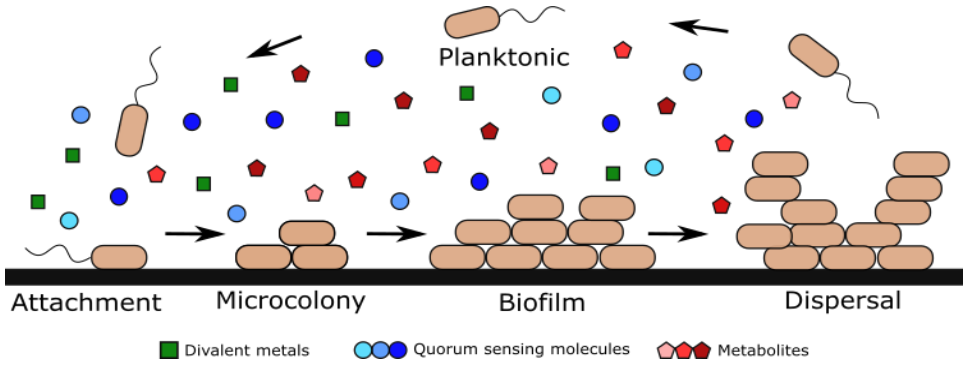

Figure 1: Biofilm Formation. Biofilm formation allows for virulence and resistance to antimicrobial agents and host defense systems because of an up-regulation in resistance genes. Various signals, such as iron, quorum sensing molecules and metabolites, report to the *P. aeruginosa* cells about the surrounding kin and host cells. These allow the *P. aeruginosa* to initiate a group response.

Host-Microbe Interactions

As the host system initiates its own immune response to relieve its self of the infection, the bacteria cells express genes to adapt to these host responses, such as phosphate starvation, oxidative stress, and host-driven cell stress.[7] Phosphate starvation interrupts the phospho-relay of signaling systems. To compensate, the phosphate is collected and stored. Phosphate starvation causes a flight response, as the bacteria increase motility.[8] It can also induce a fight response, where lethal

amounts of ferrous iron are deposited into the host cytoplasm.[9] When *P. aeruginosa* encounters phosphate starvation, the hierarchy system of QS system changes.[7, 10]

Environmental oxidative stress, caused by the host or biofilm density, signals for the secretion of extracellular hydrogen cyanide (HCN), which is toxic to the host system. The anaerobic transcriptional regulator Anr is activated when oxygen levels are low, transcriptionally-activating the HCN synthesis pathway. Anr regulator is implicated in 25% of quorum sensing- controlled virulence genes, indicating *P. aeruginosa* is able to remain virulent under anaerobic conditions.[7]

Host-derived-stressors include defense mechanisms and natural by-products of healthy cell systems, causing the upregulation of quorum-sensing systems, or microbe virulence responses such as transcriptional activation of toxin production.[11-13] Each host-derived stressor the bacteria encounters cause a response from *P. aeruginosa*. Some stressors cause an upregulation of quorum sensing systems;[13] others cause a virulent response, such as influencing genes involved in lipid modification, adhesion and motility.[12]

Quorum Sensing

Quorum sensing is a communication mechanism between bacteria within the same family or between an established bacterial community and an invasive member of a different family. Bacteria use this method of communication to induce group behavior responses, and ultimately act as a multicellular organism (Figure 2). There are three levels to quorum sensing: intra-species, intra-genus, and inter-species.

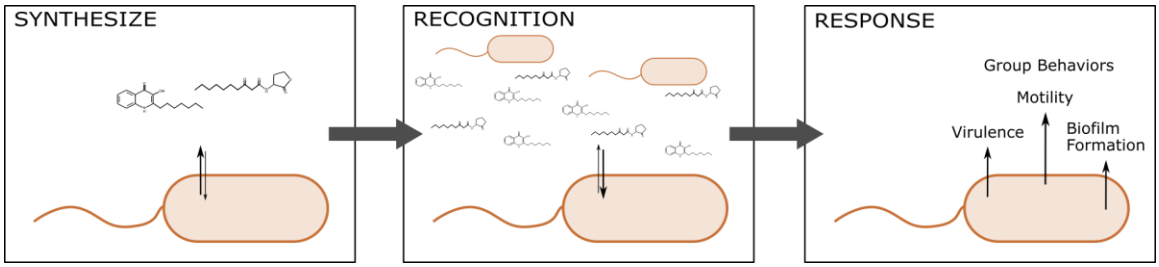

Figure 2: Quorum Sensing Communication Overview. Left panel) *P. aeruginosa* produces quorum sensing molecules recognized by kin. Middle panel) *P. aeruginosa* recognizes influx of quorum sensing molecules in its environment. Right panel) *P. aeruginosa* produces a group-response to the signal detected.

Each gram-negative intra-species quorum sensing systems contain: a small molecule synthetase and a receptor transcription factor that binds this small molecule. These small molecule synthetases can be species-specific, allowing the bacterium to differentiate same-species from different-species organisms. The receptor transcription factor can then bind only its own unique small molecule to induce gene expression. *P. aeruginosa* has four hierarchically-arranged synthetase-receptor pairs. The *las* system is the first activated when kin bacteria are near, which in turn actives the *rhl, pqs,* and *iqs* systems, each named after its respective small molecule receptor protein.[7] The *pqs* system and *rhl* system each regulate the other's productivity; while the *iqs* system can positively regulate both the *pqs* system and *rhl* system.[7] Each system also actives genes related to virulence, biofilm formation, and host system defense.[7] This is briefly summarized in Figure 3.

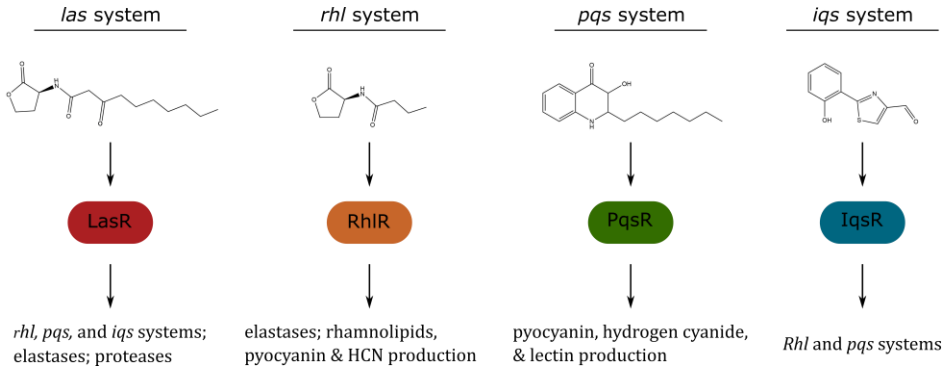

Figure 3: Four quorum sensing systems of *P. aeruginosa*. Each QS system is activated by a specific molecule to regulate genes influencing virulence, biofilm formation and host-microbe interactions.

In the *las* system, the small molecule is 3-oxo-C12 aryl homoserine lactone (OdDHL), and its synthetase and receptor transcription factor are LasI and LasR, respectively.[5] This system is responsible for activating the other quorum sensing systems, as well as extracellular elastases and proteases.[1, 7] In the *rhl* system, the small molecule is butanoyl homoserine lactone (BHL), and its synthetase and receptor transcription factor are RhlI and RhlR, respectively.[14] This system also employs proteases, in addition to rhamnolipids and pyocyanin.[1, 7] In the *pqs* system, the pqsABCD operon controls the synthesis of 4-quinolone small molecule, 4-quinolone (PQS), which is received by the receptor PqsR.[15] This system upregulates the rhl system, rhamnolipids and pyocyanin productions, as well as genes for lectin synthesis.[1, 7] The small molecule 2-(2-hydroxyphenyl)-thiazole-4-carbaldehyde (IQS) is produced by the ambBCDE synthesis operon and sensed by the IqsR receptor protein. [7] The *iqs* system interprets the environmental stress and responds by upregulating the other three quorum sensing systems.[1, 7]

Two-component systems

In addition to quorum sensing systems, *P. aeruginosa* utilizes two-component regulatory systems (TCS) to survive and thrive in a host by detecting the extracellular environment and producing an appropriate response to control the survival of itself through gene transcription. Two-component systems are the most common multistep signaling pathways in bacterial species.[16]

Two-component systems are comprised of a histidine kinase (HK) and a response regulator (RR). When the sensory domain of the HK senses a stimulus factor, the histidine kinase autophosphorylates at the conserved histidine residue from ATP in its catalytically active domain. The labile bond between the phosphorus of the phosphate and the nitrogen of the histidine is then broken as the phosphoryl group is transferred to the aspartic acid on the receiver domain of the response regulator.[16] The phosphate causes a conformational change in the receiver domain permitting dimerization with another phosphorylated response regulator in its active state. This change recruits the effector domains of the RR closer for propagating the signal. Together, the dimer acts as a transcription factor for gene regulation, as diguanylate cyclase or phosphodiesterase, or as mediators in protein-protein interactions.[16]

Many of these TCS do not work independently, but in a complex network. In some networks, sensor-kinase hybrids act upon each other, influencing the downstream phosphorylation pathway. In others, multiple histidine kinases (HKs) can phosphorylate many response regulators, and multiple response regulators (RRs) can be phosphorylated by different kinases; meaning it is not a 1:1 ratio of histidine kinase to response regulator. There are also multiple HK/RR pairs that

regulate a single gene expression. This allows the network to make a balanced decision for the biofilm's outcome.[17, 18] (Figure 4)

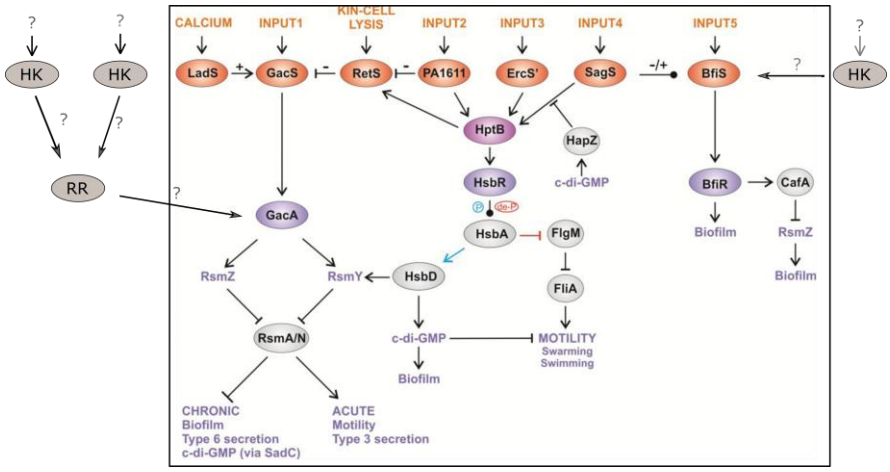

Figure 4: Complex Networks of Two-component Systems. The GAC pathway (boxed) is an example of the complex nature of two component systems. Histidine kinases are orange; response regulators are purple; and mRNAs are grey. The HKs LadS and RetS both act upon HK GacS to regulate the GacSA pathway. HKs PA1611 and ErcS' both regulate the same RR, HptB. There are still HK/RR pairs that are not characterized, and their roles in the complex TCS network are unknown (grey TCS outside GAC pathway.) Figure from Francis *et al* 2017; *Copyright © 2017, Oxford University Press*[17].

More than 60 different histidine kinases have been implicated in the formation of biofilm and virulence of *P. aeruginosa*. These TCS activate virulence genes, motility genes, fitness genes, and biofilm genes.[17, 18] For most, the inputs and outputs remain uncharacterized, and their regulation during the *P. aeruginosa* life cycle is poorly understood.[17]

The GAC pathway is a well-studied network of TCS: these systems work together to determine if the cell should make the switch from an acute infection to a chronic infection.[17, 19] This system and others like it, i.e. fimbriae formation by the ROC pathway, chemo-sensing system by the WSP pathway, are key targets to understand host-microbe interactions and microbe chronic infections.[17] Probing the

sensing activity of these signaling pathways will elucidate how, when and why the bacteria create chronic infections in a host organism.

Two-component system PhoPQ as a model system for biosensor design

The two-component system PhoPQ is thought to be responsible for biofilm formation because it increases antimicrobial resistance of the cell. The PhoPQ system is composed of the histidine kinase PhoQ and the cognate response regulator PhoP. The extracellular DNA secreted by host cells and by kin cell death chelates the magnesium from stabilizing the lipopolysaccharide (LPS) in the cell membrane, inducing cell lysis.[20, 21] However, this kin lysis allows the rest of the biofilm cells to set up a defense mechanism to the chelation effects of eDNA in the biofilm matrix.[21] When low magnesium is sensed through the sensory domain of PhoQ, the RR PhoP regulates genes responsible for LPS modification.[22] This modification of 4- aminoarabinose to the LPS adds a layer of protection from the disruption by antimicrobial peptides secreted by host systems or antibiotic drugs prescribed by doctors.

PhoQ detects magnesium, as well as calcium and peptides through an N-terminal PhoQ-DcuS-CitA (PDC) fold sensory domain.[23, 24] In an environment with high magnesium concentration, PhoQ is primarily in its kinase-inactive (or OFF) state. In low magnesium concentration environment, PhoQ is in its kinase-active (ON) state resulting in autophosphorylation of PhoQ. PhoQ then transfers its phosphate to its cognate response regulator PhoP. Phosphorylation triggers dimerization of PhoP and binding to DNA, promoting the transcription of virulence genes.[17] (Figure 5)

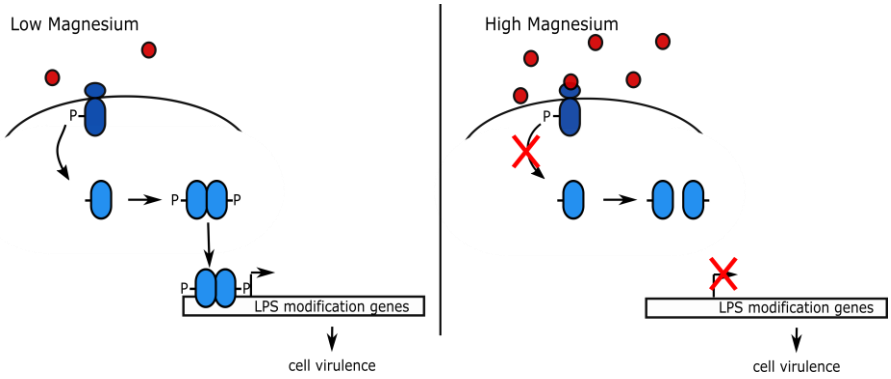

Figure 5: Two-component System PhoQP. Left) In a magnesium limited environment, the PhoQP system is active to promote cell virulence. Right) In an excess of magnesium, the PhoQP system is inactive.

New tools are needed to relate the environmental factors on biofilm formation

For the past two decades, research groups have elucidated early signaling systems that promote the transition to chronic infection. The multiple complex networks of signaling systems makes resolving environmental impacts in a temporal and spatial manner difficult. Technology that can measure individual signal impacts throughout the lifecycle of a heterogeneous biofilm would be beneficial in tracking how and when the biofilm responds and resists to the host. We aim to develop multiple methods to track the signaling activity of two component systems *in vivo* to report on the host-microbe interactions. Here, I propose two tools to report on the fluctuation of two component system activity.

We plan to test the developed biosensors in the context of developing biofilms on the surface of epithelium cells (Figure 6). We will do this in collaboration with Jennifer Bomberger's lab, who focuses on the mechanisms of initiation of biofilm formation, The Bomberger lab uses a closed system, live-cell micro-observation chamber in conjunction with a microscope to visualize the host-microbe interface.[25]

In this method, epithelial cells are grown on a microscope slide through incubation in growth media in the chamber. The bacterial cells are then injected into the chamber and given time to attach to the epithelial cell layer. Microscopy allows real-time visualization of interactions occurring within the host-microbe interface. Upon demonstration of two-component system biosensor capability in the Childers lab, we can apply the technology more broadly in the micro-chamber to visualize the spatial and temporal activity of the two-component systems with in the host-microbe interface.

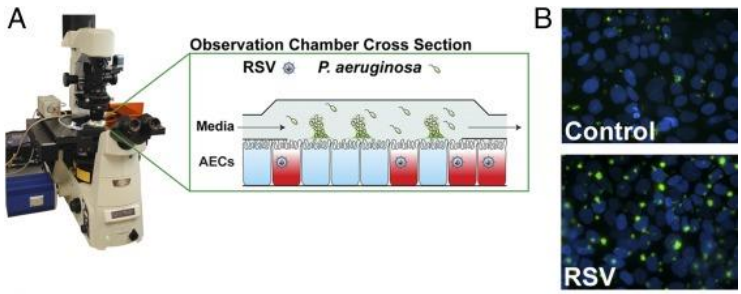

Figure 6: Figure from Hendricks *et al.*[25] A) The set up for closed system, live-cell biofilm imaging and a cross-sectional view of the micro-observation chamber. The chamber allows thermal control and media flow over cells. B) *P. aeruginosa* biofilms imaged by GFP fluorescence after 6 hours of growth on airway epithelial cells, stained in blue. Here the Bomberger group studied the effects of secondary bacterial infections on biofilm formation.

Current Tools

The interplay of host and microbes in chronic infections presents complex, heterogenous compositions that can be challenging to investigate by bulk measurements alone. Conventional molecular biology approaches to determine cellular genetic and proteomic information typically rely on cell lysis. Microscopy techniques allow for spatial and temporal determination of cellular information in the context of a living cell. Development of fluorescent tools for labeling proteins and

small molecules and fluorescent probes for studying the dynamics of the cellular functions has allowed the *in vivo* microscopy methods to continually expand. The study of host-microbe interactions involves understanding the transient and localized inter- and intra- cellular processes occurring between the host and the invader. Fluorescent sensors have been developed to track and control the biological processes has been a large focus of the field. In this section, I aim to review broad fluorescence technologies that could be employed to investigate the interactions between host and microbes.

Small molecular fluorescent sensors

Small molecule fluorescent sensors have been well studied and characterized for transition and heavy metals.[26-28] The import, efflux, and function or toxicity of these ions have been studied with fluorescent sensors with spatial control. The fluorescent sensors are typically organic molecules that interact with an ion in either an active or passive manner. During active sensing, the small molecule sensor complexes with the metal ion in its ground state, resulting in fluorescence. During passive sensing, the small molecule sensor requires a photophysical reaction between the sensor and the metal ion to cause fluorescence of the small molecule sensor.[26] The advantages of the small molecule fluorescent probes are their low molecular weight and the availability of organic compounds with the necessary chemical and photophysical properties.[28] The choice of sensor for experimental design must consider the bioreactivity, stability, solubility, selectivity, the excitation and emission maxima, and the sensitivity.[28]

Iron is a highly coveted metal during bacterial infections of a host organism. The host tightly regulates iron because it is utilized in various cellular processes, both during homeostasis and while invading a host system. Opportunistic bacteria, like *P. aeruginosa*, synthesize and secrete siderophores to scavenge iron from the host system. The Mislin group synthesized brightly fluorescent siderophore sensors to investigate the iron uptake mechanism. The fluorescent siderophores are engineered from the native siderophores and therefore, can be imported into the cell via the native siderophore-uptake mechanism. The sensors responded fluorescently to iron *in vivo*, as displayed in Figure 7. [29]

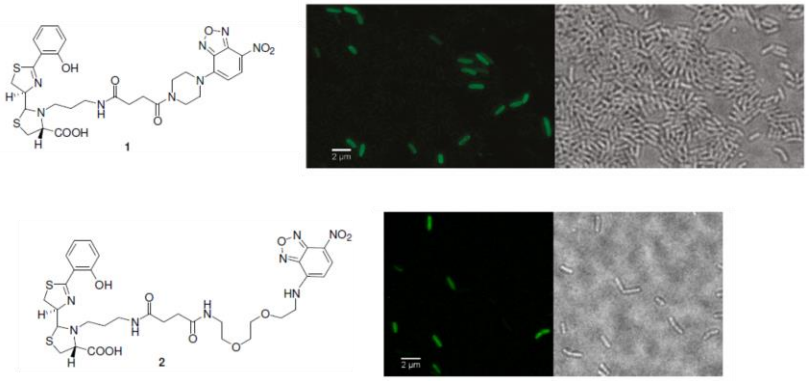

Figure 7: Iron-dependent fluorescent sensors synthesized from siderophore. Two synthetic fluorescent siderophores (labeled 1 and 2) were each incubated with P. aeruginosa and excess iron to demonstrate the bacterial uptake of the synthetic siderophores and the iron dependent fluorescence.[29] Reprinted with permission from Synthesis of Fluorescent Probes Based on the Pyochelin Siderophore Scaffold Sabrina Noël, Laurent Guillon, Isabelle J. Schalk, and Gaëtan L. A. Mislin *Organic Letters* **2011** *13* (5), 844-847; DOI: 10.1021/ol1028173. Copyright 2011 American Chemical Society.

Genetically encoded fluorescent sensors

Genetically encoded fluorescent sensors are protein-based, therefore a method of DNA incorporation, such as transformation, and expression into cell lines, is required. Although genetically encoded sensors must utilize the resources provided by the cell for transcription and translation, the genetically encoded sensors can

detect a wider variety of signals than small molecule sensors because native signaling pathways are available to use for signaling detection. There are two categories of genetically encoded sensors: sensors that control the fluorescence of a fluorescent protein (single FP sensors)[30] and sensors that rely on Förster resonance energy transfer (FRET) from a donor FP to an acceptor FP[31].

The single FP sensors utilize the pliability of the FP chromophore's stability by designing two states for the sensor that cause a drastic change in the chromophore's environment and stability. A variety of fluorescent protein variants have been used in single FP sensor designs, such as circularly permuted FP[32], and split FP[33]. Single FP sensors are intensiometric, meaning upon a binding event or a conformational change a change in fluorescence intensity occurs providing a readable output of the events that occurred.[30] One drawback of this strategy, is that fluorescence can also be affected by the concentration of the sensor and the concentration of native proteins.[34] Another major challenge with single FP sensors is in the protein engineering of a chimera between the fluorescent protein and the protein(s) of interest. This includes protein engineering decisions of insertion site and selection of linker lengths and compositions. However, many biosensors have been published despite this rational design engineering trouble.

RNA-based fluorescent sensors

Riboswitches are partially unstructured mRNA segments that bind small molecule metabolites to regulate their gene expression. One such riboswitch was found to bind fluorophores similar to that of fluorescent proteins. When bound to the

mRNA, the fluorophores fluoresce; however, if they are not bound, there is no fluorescence.[35] The Jaffrey group designed riboswitches to bind both a fluorophore (Spinach) and a small molecule metabolite, creating riboswitch fluorescent biosensors (Figure 8).[36] These are genetically encoded sensors that can bind metabolites with high specificity and selectivity of the native riboswitch. Using native riboswitches makes this sensor design modular by incorporating the Spinach stem in sequence with the native aptamer, such that the binding of the small molecule allows formation of the fluorophore. The sensors detect and report the dynamic changes of the small molecule in the cell, as well as report on agonistic or antagonistic action on the small molecule binding pocket of the aptamer. Spinach riboswitch sensors are a class of RNA-based single fluorophore sensors that utilize the native affinity and selectivity for small molecules seen in natural riboswitches. The riboswitch sensors allow temporal resolution that other detection methods wouldn't allow, i.e. using an aptamer to alter GFP expression based on metabolite concentrations.[36]

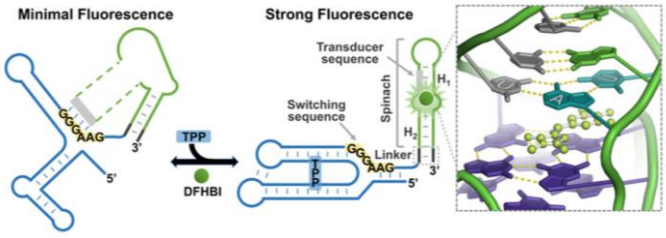

Figure 8: Structure-guided design of a small biomolecule Spinach riboswitch. The small molecule (TPP in this example) binding releases the transducer sequence (gray), allowing the formation of a critical helix in Spinach (green). The helix is critical for Spinach to bind the fluorophore (green ball) and activate the fluorescence.[36] Figure from You *et all* (2015).

The Hammond group applies this technique to create sensors for second messengers.[37, 38] Cyclic di-GMP is a second messenger that mediates cellular signaling pathways, including biofilm formation, motility and virulence. Studying the dynamics

of this second messenger, as well as others like cyclic di-AMP and cyclic AMP-GMP, will elucidate their role in particular pathways. The Hammond lab created a cyclic di-GMP sensor using Spinach riboswitch (Figure 9A).[37] The naturally occurring cyclic di-GMP binding aptamer, GEMM-I was fused to the second stem loop of the Spinach riboswitch. This fusion riboswitch, called Vc2, has high selectivity to cyclic di-GMP (Figure 9B).[37] The group has also published riboswitch sensors for cyclic di-AMP-GMP[38] and for both cyclic di-GMP and cyclic di-AMP-GMP[37]. Two methods were used to design the riboswitches into sensors: fusing native ligand-binding aptamers to Spinach or creating selectivity through mutations in the ligand-binding aptamers in an established Spinach riboswitch, respectively. The Spinach riboswitches will allow for the changes in second messengers to be quantified in different cellular stressed conditions. Sensors for a variety of second messengers will clarify the complexity of cellular processes involved in biofilm formation. However, the genetically encoded riboswitch requires the addition of the exogenous fluorophore for biosensor activity.

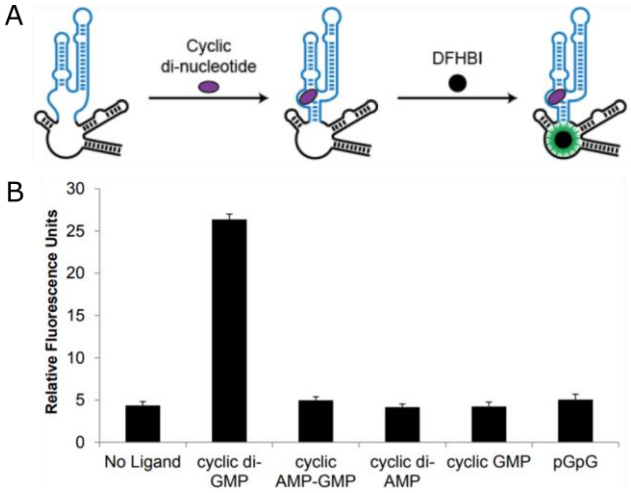

Figure 9: RNA fluorescent biosensor of cyclic di-GMP. A) Cartoon design of Vc2 riboswitch biosensor which is a fusion of the native cyclic di-GMP- binding aptamer (blue) and the fluorescent Spinach aptamer (black). With both the second messenger and the fluorescent molecule DFHBI present, the biosensor will fluoresce. B) The Vc2-spinach biosensor is selective with high affinity to cyclic di-GMP over other second messengers and small molecules.[37] Reprinted with permission from RNA-Based Fluorescent Biosensors for Live Cell Imaging of Second

Messengers Cyclic di-GMP and Cyclic AMP-GM; Colleen A. Kellenberger, Stephen C. Wilson, Jade Sales-Lee, and Ming C. Hammond; *Journal of the American Chemical Society* **2013** *135* (13), 4906-4909; DOI: 10.1021/ja311960g. Copyright 2013 American Chemical Society.

Biomolecular Fluorescent Complementation (BiFC)

In the early 2000, Biomolecular Fluorescent Complementation (BiFC) was a fluorescent protein strategy developed based upon the idea of reformation of a fluorescent protein from two non-fluorescent fragments. The fragments of the fluorescent proteins are fused to protein partners that associate or interact, allowing the visualization of the protein-protein interaction and the subcellular localization (Figure 10).[39] BiCF assay does not require complex data processing or correction for fluorescence overlap. This method also does not disturb native pathways and can allow detection of interactions of a subpopulation of a protein.[40, 41] The BiFC method also enables detection of interactions at native concentrations of the proteins, therefore not causing stress to the cell.[41]

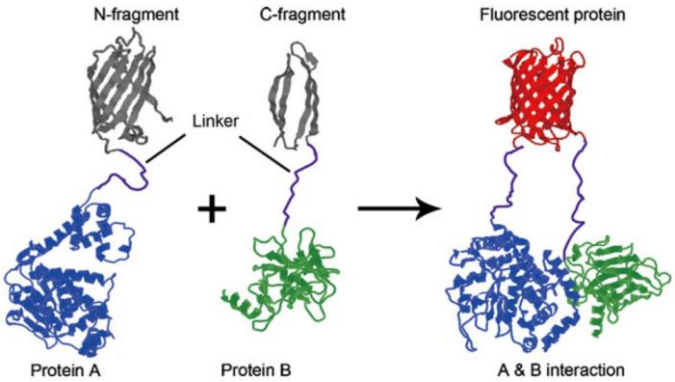

Figure 10: Schematic of the biomolecular fluorescent complementation system. A pair of interacting proteins A and B are fuses to the terminus of a fragment of RFP; when the protein pair A and B interact, the two RFP fragments associate to reconstruct RFP, producing a fluorescent emission.[39] Figure from Fan *et al* 2007*;* Copyright © 2007 Elsevier Inc.

The Verkhusha group designed a BiFC with iRFP, made from the phytochrome, RpBphP2.[42] The poor chromophore maturation of fluorescent proteins in certain cell

lines, the tendency to self-associate and the lack of high contrast red spectrum fluorescent proteins led the Verkucha group to use a phytochrome as a template for new fluorescent protein design. iRFP, has been shown to have high *in vivo* fluorescence and utilizes endogenous concentrations of biliverdin chromophore to fluoresce.[43] To create BiFC fragments, the iRFP was split at a disordered loop between the GAF and PAS domain, called iSplit. The Verkucha lab tested the ability of the two iRFP fragments to reform into the fluorescent iRFP by two methods: with dimerization coils (labeled E and K) and the known protein-protein interaction pairs, FRB and FKBP (Figure 11 A, B). The only conditions that allow formation of iSplit and fluorescence by the coil K-GAF and PAS-coil E domains are when the coils are present to interact, causing the iSplit fragments to reform the fluorescent structure (Figure 11 C, bars 1-4). To further demonstrate the functionality of the iSplit system, the iSplit system was combined with commonly used chemical induced dimerization systems (FRB/FKRB). The introduction of rapamycin to the PAS-FRB and FKRB-GAF fragments causes the dimerization of FRB and FKRB. And therefore the iSplit can reform and fluoresce (Figure 11 C, bars 5-6).[42]

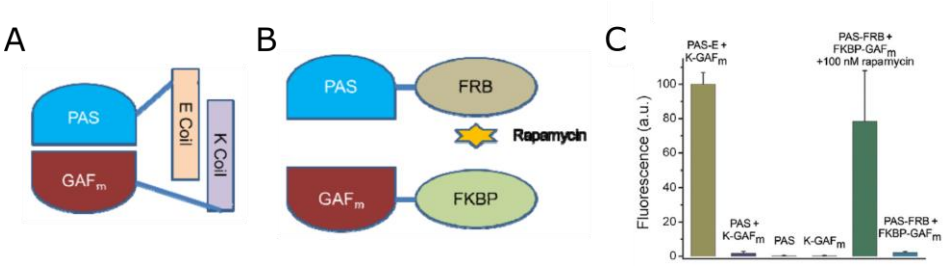

Figure 11: iSplit technology. A) Schematic of iSplit: the PAS and GAF domains fused to dimerization coils K and E to assay the ability of the PAS and GAF domains to reform fluorescent iRFP.[42] B) Schematic of PAS and GAF domains fused to rapamycin-dependent association proteins FRB or KKBP to assay the ability of inducible interaction and reformation of fluorescent iRFP.[42] C) Fluorescence brightness of the iSplit designs: the iRFP reformed and fluoresced only when both fragments, PAS and GAF, have dimerization coils K and E attached (first bar), and it doesn't not form without the dimerization coils (second bar); the iRFP could only reform when rapamycin was present to dimerize the FRB and FKBP domains (last two bars). [42] Figure from Filonov *et al* 2013. Copyright © *2013 Elsevier Ltd.*

Genetically encoded sensors also commonly employ FRET as a readout. FRET sensors typically consist of two fluorescent proteins and followed by a recognition domain, forming a single polypeptide chain. Ligand binding or cleavage of the recognition domain changes the polypeptide's conformation, resulting in a change in the relative distance and/or orientation of the two fluorescent proteins' geometry. This conformational domain variation causes a change in FRET, which is defined as energy transfer between two chromophores as a result of long-range dipole-dipole interactions.[31] Most FRET sensors fall under two categories: a single recognition domain (i.e. caspase recognition domain) and ligand-induced domain-domain interactions (i.e. calcium mediated interaction between peptide M13 and calmodulin). A new class of FRET sensors is constructed with self-associating fluorescent domains that dimerize in one state, that can be disrupted upon a ligand-induced conformational change in the recognition domains creating mutually exclusive switches between states. FRET sensors with low signal-to-noise and high dynamic range have been successfully made to detect a wide range of ions, small molecules, enzyme activities, and membrane potential.[31]

As mentioned above, second messengers are involved in regulation of cellular processes by binding to different types of receptors, riboswitches, and transcription factors. Because of this, it is important for the cell to temporally and spatially control the use of second messengers. Christen *et al.* designed a cyclic di-GMP FRET sensor to study the dynamics of this second messenger in the cell cycle process of cellular division (Figure 12A).[44] The FRET sensor is a chimera of YcgR, a cyclic di- GMP binding protein, and two fluorescent proteins, CFP and YFP. The binding of cyclic di-

GMP to YcgR induces a conformational change, resulting in the separation of the fluorescent proteins and a decreased FRET signal. The FRET signal is uniform throughout in pre-divisional *Pseudomonas* cells, indicating levels of cyclic di-GMP are homogenous. After division, there is an asymmetric distribution of FRET signal, with higher FRET signal in the parent cell and lower FRET signal in the daughter cell (Figure 12B). There is a higher concentration of cyclic di-GMP in the daughter cell. The cyclic di-GMP FRET sensor determined that fluctuations of the second messenger are cell cycle dependent.

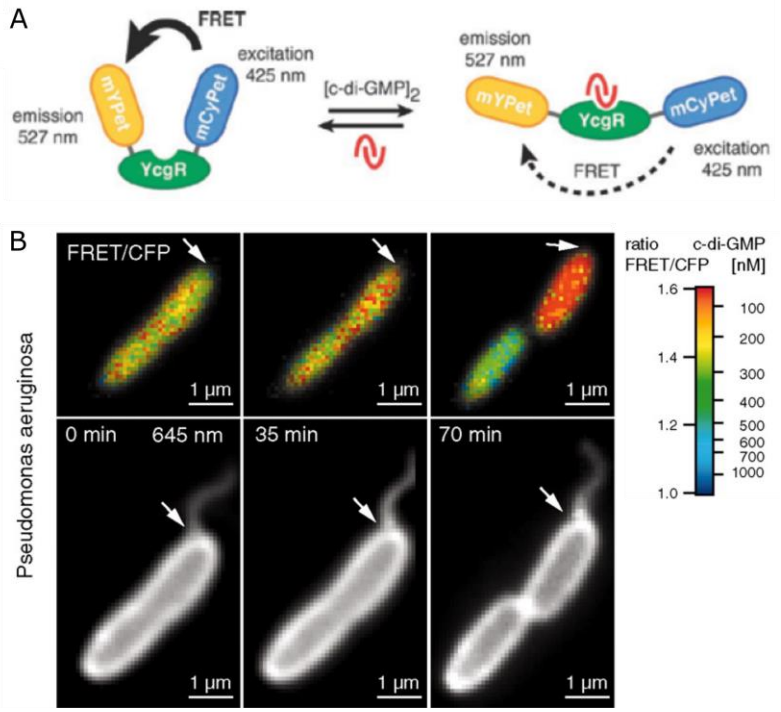

Figure 12: Second Messenger FRET studies. A) Cartoon of the cyclic di-GMP FRET sensor. The absence of cyclic di-GMP allows for high FRET signal of the fluorescent proteins. Upon binding of cyclic di-GMP to its receptor YcgR, the fluorescent proteins are no longer in proximity and there is a decrease in FRET signal. B) Cyclic di-GMP distribution in a dividing *P. aeruginosa* cell by FRET ratio from the cyclic di-GMP FRET sensor. The arrows on the images indicates location of flagellum on the parent cell.[44] Figures from Cristen *et al* 2010. Copyright © 2010, American Association for the Advancement of Science

FRET sensors are highly valuable because the fluorescence emission is independent of the concentration of FRET sensors expressed. However, designing FRET sensors is still a trial and error approach. First, the choice of fluorescent proteins has been found to greatly affect the quality of the FRET sensor.[31] The fluorescent protein domains are not exchangeable within a FRET sensor, as well as some FRET pairs have higher emission ratios because of FP-FP interactions. Second, despite homology between recognition domains, they are not easily exchanged without extra rounds of linker engineering, although groups have developed methods to modulate the design of FRET linkers.[45] FRET sensors also limit the available fluorescent proteins for multi-colored *in vivo* imaging.

To expand the use of the FRET sensor designs, researchers have been exchanging the FRET fluorescent protein pair with other fluorescent outputs, effectively making intensity-based sensors with minimal design change (Figure 13). The Zhang group exchanged the FRET fluorescent proteins of three FRET sensors, AKAR3ev, EKARev, and ICUE, with the dimerization-dependent red fluorescent proteins.[46, 47] The dimerization-dependent red fluorescent protein pair consist of a fluorescent protein pair containing a fluorescent FP-A and a non-fluorescent FP-B; the dimerization of the monomers FP-A and FP-B result in an increased FP-A fluorescence intensity.[46] This exchange of fluorescent domains created a monochrome, intensity based sensor, which allows the sensor to be used in a multi-colored imaging experiment.

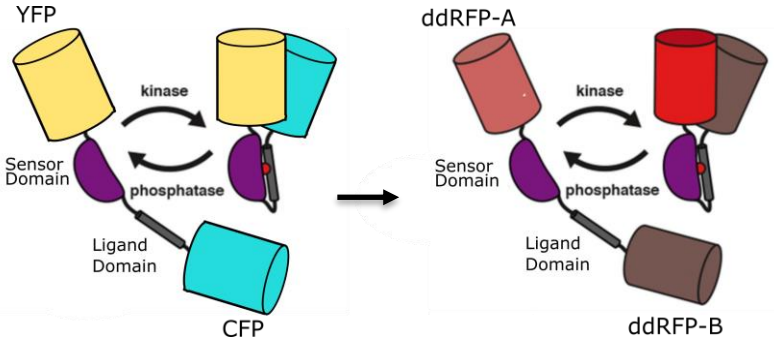

Figure 13: Schematic of fluorescent protein domain swapping. On the left is the AKAR3ev FRET sensor with YFP and CFP domains. On the right, the YFP and CFP were exchanged with ddRFP-A and ddRFP-B, respectively to create a single-color fluorescent intensity based sensor.[47] Figure from Mehta *et al.* Copyright © 2018, Springer Nature

The Merkx group used the design of a published zinc FRET, eCALWY, sensor to create a light-responsive zinc binding protein by exchanging the FRET fluorescent protein with Vivid domains (Figure 14).[48] The Vivid domains are blue light receptors and homodimerize upon illumination with blue light. This sensor showcased the modularity of swapping input and output domains from a mutually exclusive parent design to optimize the sensor to specific needs, such as visualizing zinc with a FRET sensor versus quenching zinc for system perturbation. While VividZn required linker optimization to tune the ion binding range, the authors could use the lessons learned from the optimization of eCALWY linkers, such as mutating a Zinc-binding cystine to a serine to tune the zinc affinity.

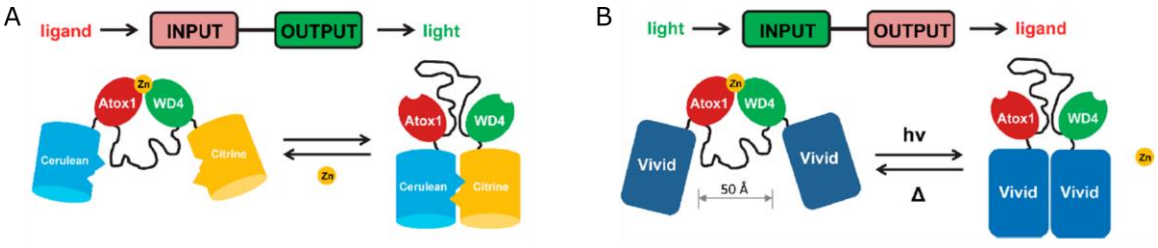

Figure 14: Schematic of FP Output Exchange. A) The schematic of the zinc FRET sensor, eCALWY. B) The schematic of the light-responsive zinc-binding switch, VividZn.[48] "Reprinted with permission from Rewiring Multidomain Protein Switches: Transforming a Fluorescent Zn2+ Sensor into a Light-Responsive Zn2+ Binding Protein." Stijn J.A. Aper and Maarten Merkx; ACS Synthetic Biology 2016 5 (7), 698-709. Copyright 2016 American Chemical Society.

The most extensively studied genetically encoded single-fluorescent sensors use circularly permuted FP (cpFP) because of the ability to attach protein domains onto the β-barrel of the FP. The conformational change of the protein domains will modulate the fluorescence of the cpFP. This approach is detailed in the subsequent section.

A relatively new and novel fluorescence technology, mentioned above, relies on dimerization of the fluorescent proteins to cause fluorescent output. This technology and its uses are reviewed and tested in a following section.

Circularly Permuted Green Fluorescent Protein Biosensors

Domain insertion of one gene into another gene is largely studied in the context of generating sensors and protein function switches. The purpose of this is to couple the functions of two individual proteins into one dual functioning protein with a distinct input and a distinct output

Figure 15).[49] Domain insertion aims to link the primary functional pathways (blue arrows) of the individual proteins, such as conformational change and phosphorylation, through a chimera fusion of the proteins (red and blue circles). The propagation of functional pathway through the protein chimera is a result of activation of the input protein from small molecule binding or protein-protein interactions (yellow circles on input protein). This functional cascade (blue arrows) leads to the output protein's activity. Domain insertion library-based approaches are advantageous because they theoretically sample every possible insertion site. This approach has successfully identified allosteric insertion sites on light-sensing domains LOV2 and dihydrofolate reductase that conserve the native function of both proteins, while coupling one protein's input with the function of the second protein's output, generating a catalytic mechanism under the control of light.[49] I propose to utilize this domain insertion concept by coupling the circularly permuted GFP fluorescence output with a native *E. coli* sensory domain as the input function.

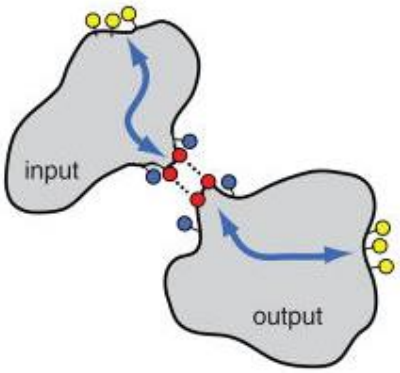

Figure 15: Domain insertion couples the functions of two individual protein domain, to create an allosteric fusion protein, with one function influencing another: input of Domain 1 affects the output of Domain 2. Figure from Lee *et al* 2008.[49] Copyright © 2008, American Association for the Advancement of Science

Circularly permuted GFP (cpGFP) was first reported in 1999.[32] The Tsien lab discovered, while altering the pH sensitivity of EGFP, a mutant variant at amino acid Y145 could tolerate a six amino acid insertion and still fluoresce. Next, they tested the circular permutation of EGFP, EYFP, and ECFP at residue 145, connecting the original N and C termini with a six amino acid linker, GGTGGS. All three circularly permuted constructs had similar fluorescence as the parent construct, but at a higher pKa. The Tsien group surveyed other sites of circular permutation by creating circular DNA of EGFP, connecting the termini with GGTGGS, and treating with DNase to create nicked strands. Ten unique constructs were discovered from this method; two of these had spectral properties indicating uniform unprotonated- chromophore excitation. One of these was Y145. In the final iteration of cpGFP, original termini of GFP were connected with a seven amino acid glycine-rich linker, GGTGGS; and the new termini were formed between amino acids N144 and Y145, where Y145 became the new N terminus and N144 became the new C terminus (Figure 16).[32]

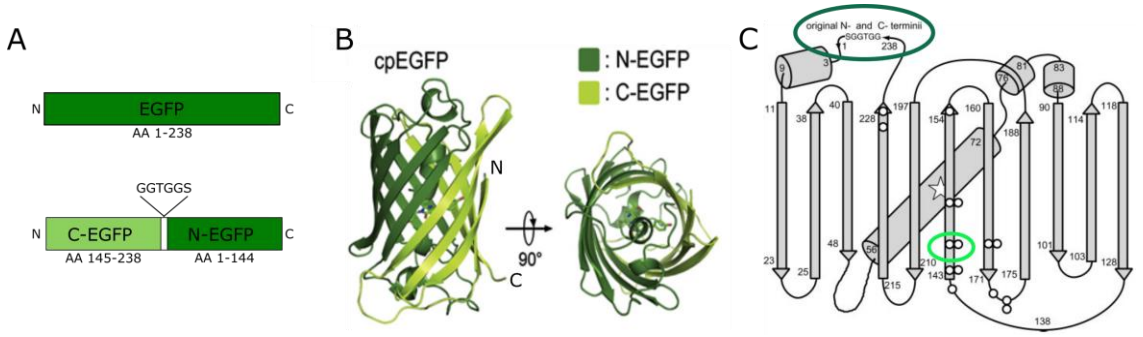

Figure 16: cpGFP Construction. A) The C-terminal half of EGFP from amino acid 145 to 238 became the N-terminal half of cpEGFP. The N-terminal half of EGFP from amino acid 1 to 144 became the C-terminal half of cpEGFP. The two halves of cpEGFP were connected by a six amino acid linker. B) The crystal structure of cpEGFP is color-coded based on the original termini halves of EGFP. The new termini of cpEGFP are labeled with "N" and "C" for the N-terminus and C-terminus, respectively. The barrel structure of EGFP is conserved in cpEGFP.[50] C) Cartoon structure of EGFP. The original termini of EGFP are connected with a linker (dark green circle) and new termini are cut between N144 and Y145 (light green circle).[32] Panel B from Akerboom *et al.*[50] Panel C from Baird *et al.*[32] Copyright 1999 National Academy of Sciences.

Circular permuted GFP fluorescent sensors detect a broad range of metabolites

Many research groups have used circularly permuted GFP fluorescence to monitor ratio changes in ATP and ADP,[51] citrate,[52] hydrogen peroxide,[53] maltose,[54] cAMP,[55] cGMP,[56] and calcium as single-fluorescent protein sensors.[50, 57-59] These fluorescent sensors are chimera proteins of cpGFP and proteins that bind the subject of interest, using a conformational change upon ligand-protein binding to create a fluorescence read out. The ADP:ATP ratio sensor is a cpGFP-GlnK1 chimera protein, where GlnK1 is the ATP binding protein with a short flexible loop in its structure.[51] This flexible loop, called the T-loop, undergoes a conformational change from a disordered structure to a compact ordered loop upon ATP binding GlnK1. The Yellen lab used rational design to insert cpGFP after each of the six residues of the T-loop of GlnK1. The same rational design was used to create the citrate sensor (CF98)[52] and hydrogen peroxide sensor (HyPer)[53] for a input sensor with circularly permuted GFP readout. The Kirimura lab used the using the apo and bound structure of CitA to

determine cpGFP insertion sites on the flexible loop sensitive to citrate binding (Figure 17).[52] HyPer sensor is a chimera of cpGFP inserted into OxyR, a hydrogen peroxide sensitive regulatory domain, in a flexible loop with localized conformational change in the presence of hydrogen peroxide.[53]

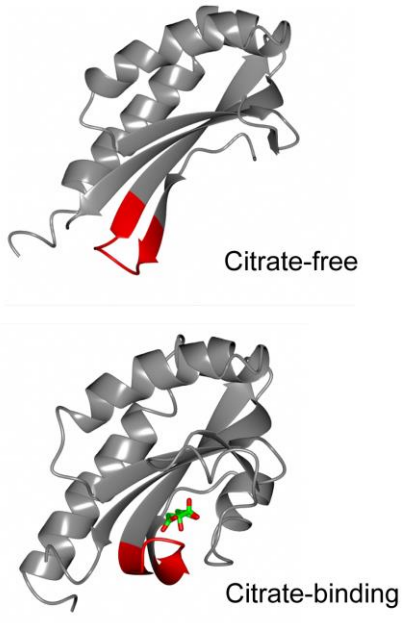

Figure 17: CitA conformational change upon citrate binding. The top structure shows the apo structure of CitA. The bottom structure shows the citrate-bound (green molecule) structure of CitA. The residues 97-105 of CitA are highlighted in red and represent the flexible region targeted for cpGFP insertion. Insertion of cpGFP at reside 98 of CitA showed high fluorescence in a citrate-dependent manor. Figure from Honda *et al.*[52]

In Kitaguchi *et al*, a cAMP sensor, FLAMINDO, was constructed with cAMP binding protein, Epac1 and fluorescent protein citrine.[55] Kitaguchi *et al* used precedence that inserting a domain into citrine at an amino acid residue (Y145) near the chromophore leads to a conformationally dependent sensor (Figure 18).[55] This creates the circularly permuted variant of fluorescent protein. To create a cAMP-dependent fluorescent sensor, the group tested 12 variations of the Epac1 and citrine fusion: altering the length of Epac1 and the length of the linker.[55] Seven variants of

the sensor with truncated Epac1 and citrine were assayed for linker length effect on fluorescence. Linkers of 2, 3, 5, and 6 amino acids were sampled between both fusion points. Ultimately, the linkers composed with 2 or 3 amino acids propagated the cAMP signal into high fluorescence.

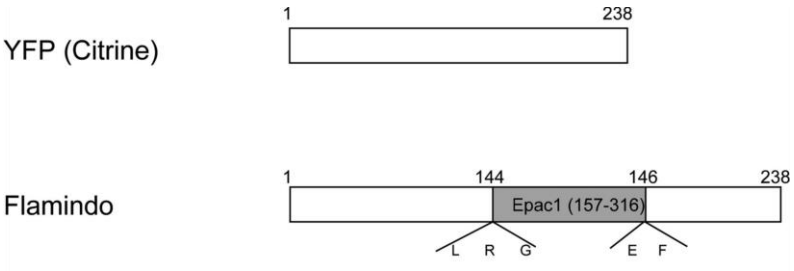

Figure 18: Schematic of cAMP sensor FLAMINDO. The cAMP binding protein was inserted in place of AA Y145 of citrine. After analysis of truncations of Ecpac1 residues 157-316 of Epac1 were sufficient for cAMP-dependent fluorescence. Figure from Kitaguchi *et al.*[55]

Design of fluorescent sensor readout of protein phosphorylation

Fluorescence sensors with capabilities of visualizing cell signaling can critically help dissect upstream, downstream, and cross talk effects of a signaling pathway upon cellular processes. The Umezawa group created a *sin*gle color fluorescent sensor to read out protein *phos*phorylation, named *sinphos*. They designed a cpGFP sensor (Figure 19) using a phosphate-accepting domain (red protein) and its phosphorylated binding partner (phosphorylation recognition domain, orange protein). A localization tag (light blue protein) was added to localize the phosphate accepting domain to the protein that natively phosphorylates the domain upon signal recognition.[60] Therefore, when the signal is present, the phosphate-accepting domain is phosphorylated and binds to the partner protein, causing a conformational change that stabilizes the cpGFP chromophore and allows fluorescence. As proof-of-concept, the *sinphos* design was applied to an insulin-

induced protein phosphorylation event in mammalian cells. In this pathway, insulin activates the insulin receptor to phosphorylate the insulin receptor substrate (IRS-1), initiating the interaction of IRS-1 and the Src homology-2 (SH2) domain of phosphatidylinositol 3-kinase. The tyrosine phosphorylation domain of the IRS-1 was used as the phosphate-accepting domain (red protein) and the SH2 domain was used as the phosphorylation recognition domain (orange protein) (Figure 19). The localization domains, a pleckstrin homology (PH) domain and a phosphotyrosine-binding (PTB) domain, localize the *sinphos* to the insulin receptor. The *sinphos* sensor is localized to the insulin receptor, allowing efficient phosphorylation on the tyrosine phosphorylation domain. The interaction of the phosphorylated domain and its binding partner, SH2, induces a conformational change in the cpFP that causes a fluorescence intensity change.

The technology to visualize cell signaling is important to understanding upstream, downstream, and cross talk effects of a pathway on the cellular processes. This monochromic protein phosphorylation sensor will contribute to multi-event cell imaging. However, there were no published difficulties in designing the sensor, consequently it is not obvious if these sensors are easy to engineer with a phosphate-accepting group and the its binding partner on the termini of cpGFP.

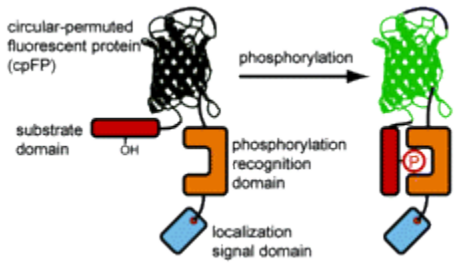

Figure 19: Design of phosphorylation sensor. The sensor has four domains: cpGFP, substrate domain, phosphorylation recognition domain, and localization signal domain. phosphorylation of the substrate domain

(red) by an endogenous kinase causes the phosphorylation recognition domain (orange) to bind to the phosphorylated substrate domain (red), which changes the fluorescence intensity of the cpGFP (green). The localization signal domain (blue) recruitments the sensor to a particular intracellular location to allow phosphorylation of the substrate domain (red). Reprinted with permission from Kawai *et al*. Copyright 2004 American Chemical Society.[60]

Design of sensors by *in silico* analysis of ligand-binding protein states

A key challenge within this field is the lack of systematic method to design the single fluorescent protein sensors with cpGFP. To address these concerns, the Looger lab developed generic strategies for construction of a maltose sensor composed of maltose binding protein (MBP) and cpGFP.[54] The insertion site of cpGFP was chosen through conformational change analysis on the crystal structures of the apo and bound form of maltose-MBP. By surveying MBP for the residues with the greatest change in dihedral angles, the Looger lab found two insertion sites for cpGFP (Figure 20). As a positive control of the sensor design, the two insertion sites previously found in MBP to create a chimera function switch were assayed alongside the insertion sites found by the *in silico* analysis.[61] Panel A of Figure 20 highlights the conformational change maltose binding protein undergoes when maltose binds. The locations of cpGFP insertion are indicated by colored spheres: the green and violet locations are the previously established insertion sites and the cyan (residues 175-176) and yellow (residues 311-312) are the *in silico* determined sites. Panel B of Figure 20 is the dihedral angle analysis of the maltose binding protein apo and maltose-bound forms. Residues 175 and 311 are label on the graph, highlighting the large change in diheadral angle compared to the two states of maltose binding protein. The Looger lab tested these insertion sites with cpGFP insertion. The linkers between MBP-cpGFP and cpGFP-MBP were optimized by a library of variants with

randomized linkers by single-stranded uracil template mutagenesis, where all 20 amino acids were tested in both positions. Several thousand variants were screened to yield three viable maltose dependent sensors: one of the insertion sites by the nonhomologous recombination method and both of the insertion sites of the *in silico* analysis.[54] These studies led to a maltose sensor that detects maltose over a range of 0.1 μM to 1000 μM; upon addition of maltose the fluorescent protein signal increased between 1-fold and 2.5 fold for two of the sensors they continued to use for analysis. The three viable sensors have a change in diheadral angles greater than 10 degrees at the point of cpGFP insertion. Based on the analysis of the linker mutagenesis, linkers cannot be predicted as the linkers of the three viable maltose sensors do not share similarities: one has two prolines linking the cpGFP to Maltose, while another has two glycines. Linker composition depends on the terminal residues and optimization of each fusion point will determine the ideal residues near the chromophore to create the largest change in fluorescent from one state to the other.

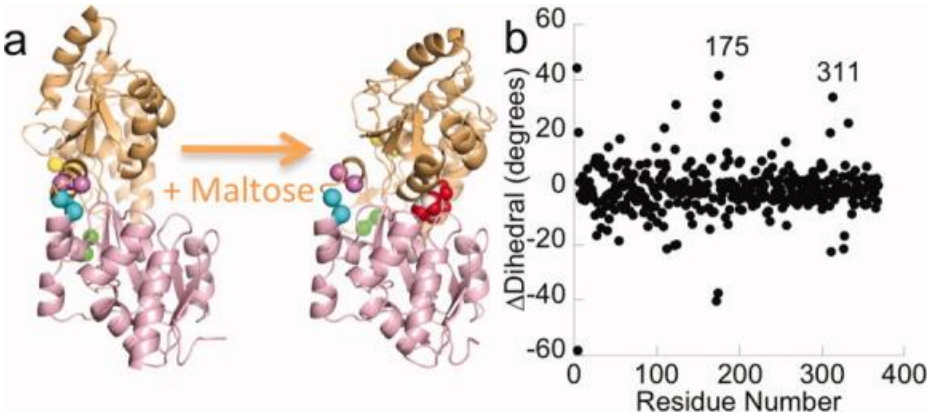

Figure 20: A) Conformational change in maltose binding protein upon the binding of maltose (red spheres). The locations of cpGFP insertion are indicated by colored spheres. B) The change in diheadral angles between the bound and apo states of maltose binding protein. The residues 175 and 311 are insertion sites of cpGFP determined by the change in diheadral method. Figure from Marvin *et al.* Copyright © 2011 Wiley - Liss, Inc.[54]

These studies take a two-step approach for sensor design that includes initially an *in silico* rational design for insertion sites by comparison of bound and unbound crystal structure dihedral angles, followed by optimization of linker composition. To further test this method, a phosphonate sensor was designed using PhnD binding domain.[62] Analysis of the bound and unbound 2-aminoethylphosphonate to PhnD domains identified four insertion sites: residues 88-90, in which the dihedral angles change the most in the apo and bound structures. The cpGFP insertion at residue 90 of PhnD yielded the highest affinity for 2-aminoethylphosphonate. A subsequent screen of linker mutants of PhnD-cpGFP linker, including deletions and insertions of residues, produced a two amino acid linker, AlaAsp between residue 88 of PhnD and cpGFP, and a two amino acid deletion, residues 89 and 90 of PhnD. These studies led to a phosphonate sensor that detects phosphonate sensor over a range of 10 μM to 100 μM, upon addition of phosphonate the fluorescent protein signal increased 1.5-fold. A drawback of this approach is that in silico insertion design disregards possible sensor domains that do not have crystal structures for either bound and unbound.

Based upon similarities between the maltose binding protein (MBP) and glutamate binding protein (GltI) the Looger lab designed a new glutamate sensor using the *in silico* insertion design method.[63] The glutamate binding protein, GltI, has only been crystalized in the bound state. They propose to overcome this by using structural similarities between MBP and GltI to choose insertion sites. By mapping the three residues identified as undergoing conformational change in MBP, a few

possible homologous insertion sites were identified on GltI. The linkers were optimized by a library of randomized linkers by single-stranded uracil template mutagenesis, where all 20 amino acids were tested in both positions After linker optimization, one of the *in silico* insertion sites yielded a glutamate-dependent sensor that detects glutamate over a range of 0.1 μM to 100 μM, upon addition of glutamate the fluorescent protein signal increased 4.5-fold.[63]

The Looger lab proved both bound and unbound crystal structures are not necessary for *in silica* design, if there are both crystal structures for a structurally similar protein. Linker composition has proved to be best determined by library screen approach. This aspect makes the design of biosensors less modular.

cpGFP linkers play active roles in chromophore stabilization

The most well-characterized engineering of a chimera sensor is the calcium sensor, GCaMP2.[50, 57, 58] The GCaMP2 sensor is composed of three domains: cpGFP, the peptide M13 and the protein calmodulin. In the presence of calcium ions, M13 peptide binds calmodulin.[57] The GCaMP2 sensor exploits this protein-protein interaction to construct a sensor for Ca^{2+} ions.

This high affinity binding interaction between the sensor and calcium changes the chemical environment around the permuted termini of cpGFP, allowing a network of hydrogen bonding to stabilize the chromophore (Figure 21). Engineering the optimal sensor for calcium required detailed attention to the linkers connecting the M13 and calmodulin proteins to the termini of cpGFP.[50, 54, 57] The Imoto Lab, the first lab to publish GCaMP2, sampled two and three amino acid linkers, in groupings of basic, acidic, and flexible, between M13-cpGFPand cpGFP-CaM. The highest calcium-

dependent fluorescence of the sensor occurred with acidic and basic linkers for M13-cpGFPand cpGFP-CaM, respectively.[57] The crystal structure of the GCaMP2 sensor depict the linkers involved in stabilization of the chromophore because the linker is faced into the β-barrel, near the chromophore (Figure 21 left).[50]

When designing the maltose, phosphonate and glutamate sensors, the Looger Lab used uracil template mutagenesis as a high-throughput screen for linkers composed of two amino acids, where each amino acid combination was screened.[54, 62, 63] They conclude that optimization of linkers between ligand-binding domain and cpGFP is necessary for each insertion site into the ligand binding domain. Their best sensors included two amino acids that are vastly different when comparing between sensors but each linker play a specific role in tuning ligand-dependent fluorescence of the sensor (Figure 21 Right).[54]

I propose the future designs of the following cpGFP biosensors will require optimization of the linkers attaching the cpGFP and the ligand binding domain. Based on the compilation of linker design data, two- amino acids linkers between the ligand-binding domain and cpGFP are sufficient to produce ligand-dependent fluorescence. I propose future sensor designs to incorporate a library method approach to optimizing linkers as the Looger lab has shown. The library linkers will incorporate each of the 20 amino acids at each position to sample all combinations of amino acid characteristics in the ability to stabilize the chromophore in a ligand-dependent manner.

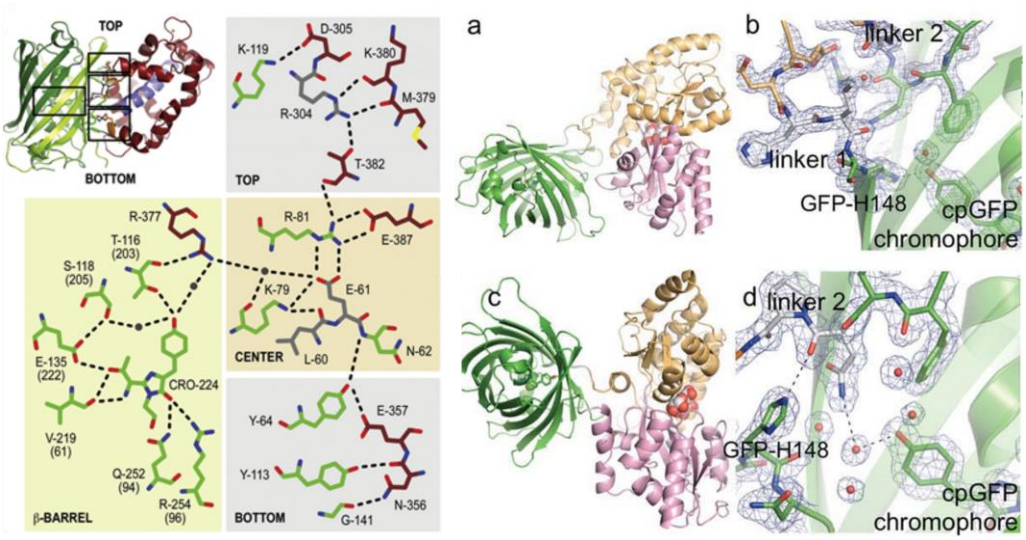

Figure 21: Linker Composition Affects cpGFP Fluorescence. Left) The GCaMP2 calcium sensor crystal structure displays the influence of the linkers (gray amino acids) on the stabilization of the chromophore.[58] Right) The maltose-cpGFP sensor crystal structure also displays the influence of the linkers.[54] Panels A and B show the crystal structure of the maltose-cpGFP sensor has a HL linker between the maltose binding protein-cpCGP fusion. Panels C and D show the crystal structure of the maltose-cpGFP sensor has a linker of NP between the cpGFP-maltose binding protein fusion. The linkers vary in amino acid composition and location in the maltose-cpGFP fusion, yet they both impact the stabilization of the chromophore. Left panel from Akerboom *et al*.[50] Right panel from Marvin *et al.* Copyright © 2011 Wiley - Liss, Inc.[54]

Using Circularly Permuted Fluorescent Proteins as a Read-out of Two Component System Activity

Two-component systems control bacterial adaption from changes in the environment by regulating gene expression. To do this, the systems sense environmental stimuli through the sensory domains of histidine kinases. Stimuli cause a signal transduction through the two-component system, from the sensory domain all the way to the response regulator that causes genetic responses. As the environment surrounding the host-microbe interface changes, it induces genetic responses to complete the transition from acute bacterial infection to chronic bacterial infection. If we study these environmental changes in the host-microbe

interface through biosensors, we can determine the best approach to inhibit the transition to chronic infection.

Many two-component systems implicated in virulence and biofilm formation have not been full characterized.[17] Most do not have defined stimuli or defined structures of the sensory domains. This makes it challenging to construct broad spectrum biosensors when the "spectrum" is undefined. I propose to utilize the well characterized sensory domain folds to do so. Many signals discussed in the *Francis et al* review of two-component systems implicated in biofilm formation, are utilized across all bacterial life.[17] All bacteria need to sense their environment to determine the possibility of surviving in an environment, therefore many of the signals *P. aeruginosa* uses to initiate the transition to chronic infection, other bacteria are also using them to influence their cellular behavior. By utilizing this cross section of known signals, I can create biosensors to respond to the stressors used by *P. aeruginosa* by utilizing the periplasmic sensory domains known to be activated. The two-component systems of *P. aeruginosa* that are known to implicate the formation of biofilm, but do not have known signals, can also be utilized as biosensors. These biosensors can correlate a known down-stream genetic response to novel spatial and temporal information within the transition to chronic infection.

The sensory domains vary within the broad family of two-component systems (Figure 22). They vary in location: extracellular, membrane bound, and cytoplasmic. They also vary in structures, such as all-helical, a mix of α- helices and β- strands (PAS, GAF, Pas-like PDC, PHY), and extracellular loops.[64] These sensors bind heme, FMN, FAD, 4-hydroxycinnamic acid, malonate, malate, and succinate, citrate, nitrate,

divalent metal cations, and the list goes on; as well as uncharacterized ligands, such as "kin cell lysis", or unknown ligands.[17, 64]

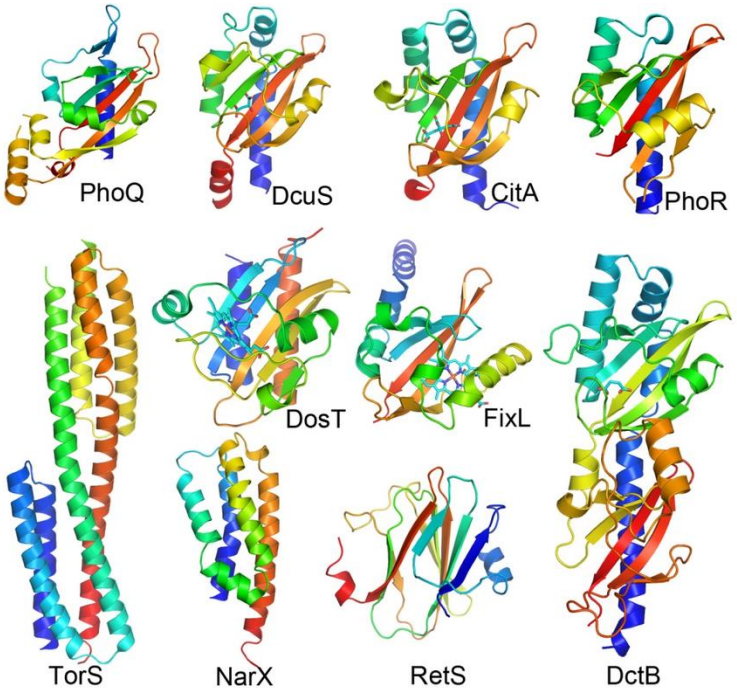

Figure 22: PhoQ, DcuS, CitA, and PhoR have PDC folds in the periplasm. DosT and FixL are cytosolic sensor domains and adopt GAF and PAS Domains, respectively. DctB has two tandem PDC domains in the periplasm. NarX is an all-helical domain, and TorS is a double all-helical domain. RetS is currently the only β-sandwich fold. If the substrate is known, and its location in the domain fold is known, it is represented in stick format. Figure from review by Wang.[65]

I propose beginning biosensor construction with the well-characterized PhoQ histidine kinase. The structural data of the PDC sensory domain of PhoQ, bound to its inducer magnesium, allows me to rationally design biosensors with the PDC domain to sense magnesium in the enviornment.[66] This first generation sensor will be designed through analysis of the PDB structure of the PhoQ sensory domain. Because of the modularity between PDC domain structures, I propose the biosensor design rules I learn from the PhoQ PDC domain will transition to utilizing other PDC domains, as well as PAS and GAF domains, in the biosensor design (Figure 23). As mentioned

previously, a citrate-cpGFP sensor was designed with the PDC domain CitA.[52] The specific location of ligand binding is unique in PDC domains, suggesting a one fusion site-fits all, however the general fold of ligand binding is conserved. The transferable information about sensor engineering, coupled with a domain insertion library approach will produce broad spectrum sensors to probe the host-microbe interactions.

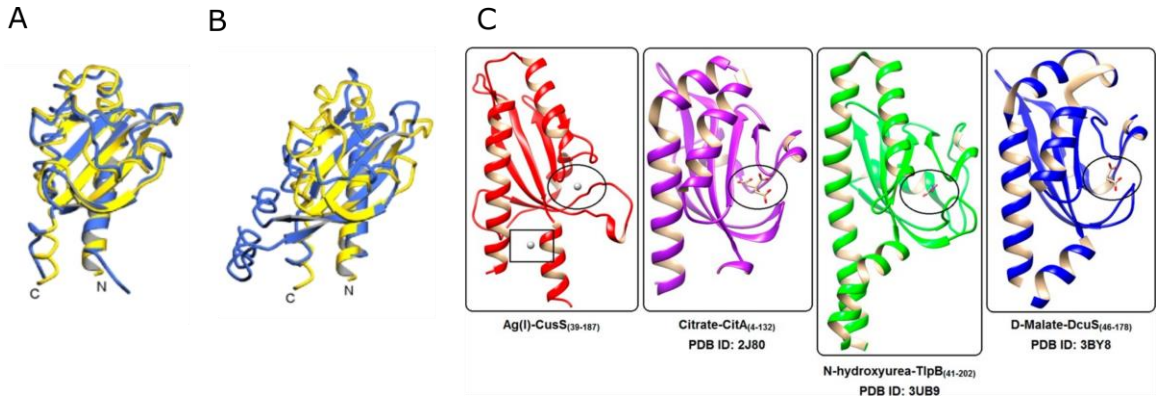

Figure 23: A) is the overlay of PDC domains of DcuS (yellow) and CitA (blue). B) is the overlay of PDC domains of DcuS (yellow) and PhoQ (blue). C) shows 4 PDC domains bound to their respective ligands, enclosed in circles and square boxes. Panel A and B is from Cheung *et al* 2008[67] and Panel C is reprinted with permission from "The Structure of the Periplasmic Sensor Domain of the Histidine Kinase CusS Shows Unusual Metal Ion Coordination at the Dimeric Interface" Trisiani Affandi, Aaron V. Issaian, and Megan M. McEvoy; Biochemistry 2016 55 (37), 5296-5306. Copyright 2016 American Chemical Society. .[68]

For this project, I have designed biosensors based upon previous cpGFP biosensors, to detect signals that regulate host-microbe interactions. I hypothesize that conformational or oligomeric changes upon ligand binding will alter the environment surrounding the chromophore and provide a fluorescence signal readout of the pathway. Success in the development of cpGFP biosensors will allow us to map the signaling landscape of host-microbe interactions and provide a deeper understanding of how these pathways orchestrate host-microbe interactions and reveal new potential antibiotic targets.

Results and Proposed Studies

I propose to use rational design of fusion sites by using the crystal structure of the PhoQ PDC periplasmic sensor domain to select locations that would not disrupt magnesium binding yet, from molecular dynamic studies, have been predicted to undergo magnesium-dependent conformational changes (Figure 26).[24, 66] The rational designed fusion sites are a first generation approach, with the purpose of developing analysis methods that will build the foundation for future library-based directed evolution approaches. With GFP as a functional readout, fluorescence microscopy, fluorescence plate reader and flow cytometry will be utilized to collect information on the input-signal dependent changes in fluorescence. The identification of functional protein insertion sites can be challenging via rational design, but with the developed analysis methods proposed here, I also plan to apply an insertion library approach to screen for functional sensors.[69]

The method of Domain Insertion Profiling with sequencing (DIP-seq) uses *in vitro* transposition to insert one domain into another domain, using the random enzymatic activity of transposases. Using flow cytometry, together with high throughput sequencing to compare low fluorescence versus high fluorescence variants, leads to a functional sensor and identification of general insertion regions within the PDC domains..[69] The work-flow for DIP-seq is presented below (Figure 24).

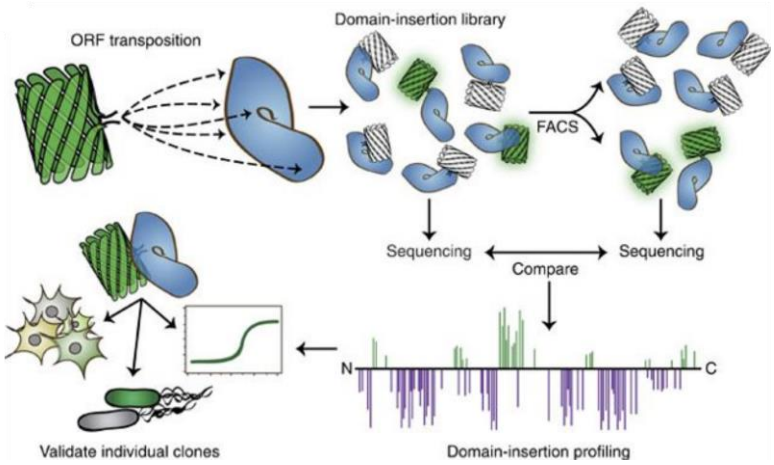

Figure 24: The work flow for domain insertion profiling library to create functional sensors. The library of fusions is created and screened by FACS and by sequencing, identifying insertion sites enriched during FACS. The productive insertion sites are assayed for sensor functionality. Figure from Nadler *et al*.[69]

The DIP approach library used a Mu transposon flanked by DNA restriction site BsaI to introduce insertions (orange block on plasmids in Figure 25) onto a library staging plasmid containing one of the protein of interest for fusion, Domain 1 (blue gene on plasmid in Figure 25). The staging plasmid vector is replaced with the expression vector by restriction enzymes. Only functional insertion domains in the open reading frame of Domain 1 will remain. Finally, using the BsaI Type IIS restriction enzyme, the second protein of interest, Domain 2, (green gene on plasmid in Figure 25) is inserted where the insertion transposon gene is positioned by Golden Gate cloning. The reaction was transformed and grown for functionality assay by fluorescent screening. The library was screened using fluorescence-activated cell sorting (FACS) to select for cells carrying plasmids with functional protein expression of protein-fusion sensor (Figure 24). The library was sequenced to compare enrichment of plasmids by FACS. The cross section of this data contained productive insertions of Domain 2 into Domain 1. Cells with functional expression plasmids were

then analyzed in 96 well plate-reader fluorescence assay in the presence of the fusion sensor's activator and inhibitor (Figure 24). This type of screen has successfully identified multiple protein-fusion sensors that responded to the activator. They constructed single fluorescent biosensors this way for maltose binding protein and D-trehalose/D-maltose-binding protein. [69]

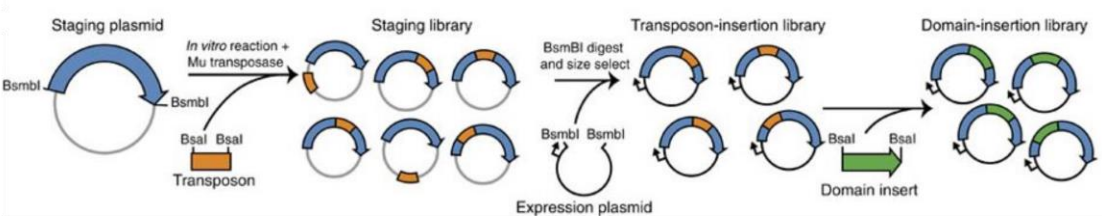

Figure 25: The work flow of creating a domain- insertion library with transposons. The transposon creates a place-holder in Domain 1. The insertions of transposon in the open reading frame of Domain 1 (blue) are selected by cloning into expression plasmid. Domain 2 is then inserted into the transposon place by restriction enzyme cloning. Figure taken from Nadler, et al.[69]

Rational Design of functional sensor domain-cpGFP fusions

To rationally design magnesium sensors, I used the crystal structure of the *E. coli* sensor domain of PhoQ (PDB 3BQ8) and bound-unbound modeling of the sensor domain.[24, 66] Magnesium ions interact with a cluster of acidic residues (amino acids: EDDDDAE) in one region of the domain and cause a conformational change in the sensor domain (magenta helices in Figure 26A).[66] The part of the domain with the acid clusters undergoes a conformational change to closer proximity to the transmembrane helices, propagating a scissoring motion through the dimerizing helixes (green helices in Figure 26A) of two PDC domains.

Fusion sites were selected where computational modeling indicates a magnesium-dependent conformational change occurs and where insertion of a large protein (cpGFP) is less likely to disrupt the sensing capabilities. I inserted cpGFP into

three sites: two sites were adjacent to the acidic cluster (sensors PDC_{114} Fusion and PDC_{115} Fusion) and one site is in a loop farther from the acidic cluster which undergoes a dramatic conformational change upon binding (sensor PDC_{55} Fusion) (Figure 26B). These designs are mimicked after the Ca^{2+} sensor[57] and maltose sensor[54] design, where the cpGFP has one domain of the ligand-binding domain on each terminus. In my designs, I chose to split the PDC domain in two smaller domains to mimic the design of ligand binding domain on each terminus of the cpGFP. This will require the N and C termini of cpGFP to be local once the PDC structure is formed. The conformational change upon binding of magnesium will drive the fluorescence as the environment surrounding the chromophore changes and stabilizes the excited state.

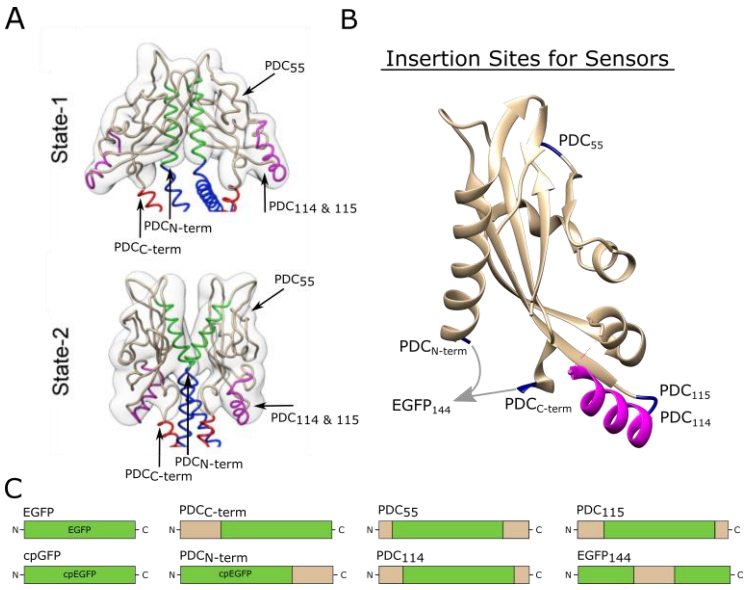

Figure 26: Labeled Structure of the PhoQ PDC Domain. N-terminal TM helices (blue), dimerizing helices (green), Mg^{2+} -binding acid residues (magenta), C- terminal TM helices (red). A) Figure from Ref. 16: State-1 is the structure of unbound PDC domain; State-2 is the structure of bound Mg^{2+}-PDC domain. The saturation of magnesium residues causes the helical wings to burry into the membrane, causing the conformational change. B) Locations of cpGFP insertion are labeled in cyan on the N-terminal amino acid of insertion site. C) Design of magnesium cpEGFP sensor. Green indicates cpEGFP unless otherwise stated. Tan indicates PDC domain of PhoQ. The numbers designate the fusion site. Panel A is adapted from Molnar *et al.* Copyright © 2014 Elsevier Ltd. All rights reserved.[66]

The N- and C- termini of the periplasmic PDC domain are both attached to transmembrane (TM) helices. When the PDC sensor detects a change in magnesium concentration, the N and C terminal helices of PDC cause the TM helices to undergo a scissoring motion.[66] Therefore, I chose to fuse cpGFP to the N- or C- termini (Figure 26). I hypothesized this scissor motion would alter the environment around the exposed chromophore in favor of stabilizing the mature chromophore. I also inserted the PDC domain into eGFP at the site of circular permutation, GFP_{144} fusion (Figure 26). I hypothesized that the scissoring motion, which pulls the termini of PDC away from each other, upon magnesium binding, will alter the environment surrounding the chromophore.

Assessment of rationally designed sensors' functionality in vivo

The sensors were tested for sensing capability through a media wash assay.[70] The wash protocol requires the resuspension of the cell pellet in M9 media without the addition of magnesium or calcium. The final resuspension was in M9 media with supplemented concentrations: 0 mM $MgSO_4$, 0.01 mM $MgSO_4$, 10 mM $MgSO_4$, or 10 mM EDTA. The following fluorescence data was collected on an epifluorescence microscope. Previous *in vivo* PhoQ activity is shown to be sensitive to Mg^{2+} concentrations between 0- 0.01 mM $MgCl_2$ and 0.01- 50 mM $MgSO_4$.[71, 72] Therefore I tested if my designed PDC fusion sensor was sensitive to $MgSO_4$ concentrations in the range of 0-10 μM.

The first control I tested using the wash assay was eGFP, which is the structural basis for cpGFP. The amount of fluorescence did not change as more magnesium was added to the media; indicating there is no effect of magnesium on the

fluorescence of eGFP (Figure 27). The average total cell fluorescence intensity values for 0 mM, 0.01 mM and 10 mM supplemented magnesium are 1107 ± 760, 1217 ± 671, and 1229 ± 704, respectively. An ANOVA test was performed between each magnesium concentration at a 95% confidence interval. The P value for this assay was >0.9999, indicating there is no significance of the variation in magnesium on the fluorescence of EGFP.

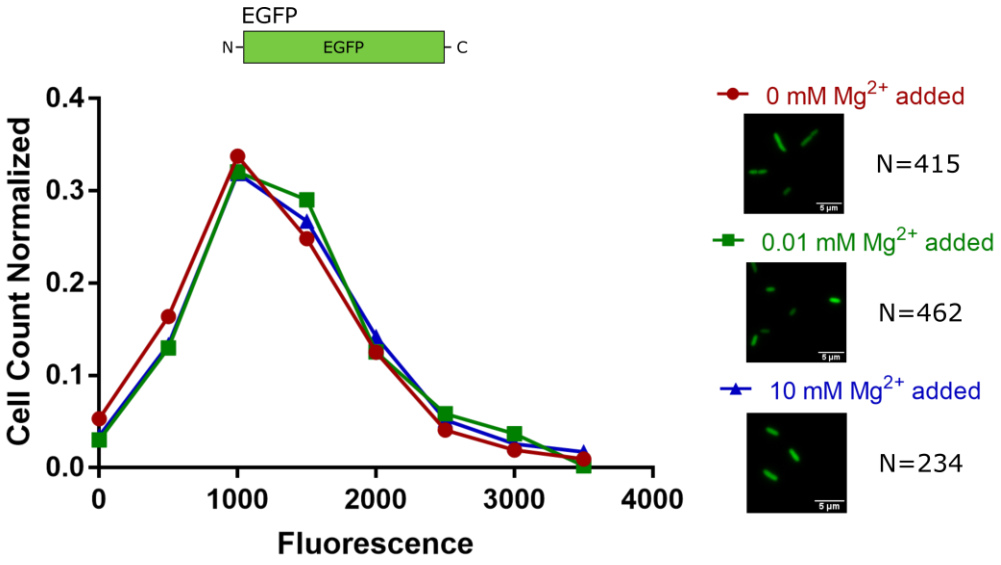

Figure 27: eGFP fluorescence at various magnesium concentrations. Left) Wash assay with media swap graph with cartoon of sensor design inset. Right) Representative cells of the wash assay and the number of cells included in the analysis.

Using the epifluorescence microscope, I tested the functionality of the $PDC_{C\text{-}Term}$ fusion sensor, where the N- terminus of cpGFP was fused to the C- terminus of the PDC domain (Figure 28). Testing cpGFP and GFP fluorescence against the effects of EDTA addition will allow me to determine if EDTA effects the fluorescence of the sensor. Titrating- in magnesium had no effect on the fluorescence (Figure 28). The average total cell fluorescence intensity values for 0 mM magnesium, 0.01 mM

magnesium and 10 mM magnesium, and 10 mM EDTA supplemented M9 are 1380 ± 460, 1835 ± 495, 1883 ± 475, 1435 ± 587 respectively. An ANOVA test was performed between each magnesium concentration at a 95% confidence interval. The P value for this assay was >0.9999, suggesting there is no significance of the variation in magnesium on the fluorescence of this sensor. Although by visualization of the data, it seems that EDTA supplementation caused less fluorescence; possibly because the free magnesium was chelated. I can optimize the M9 washes with supplemented EDTA to ensure the free residual magnesium is chelated for all media conditions. This could also mean that the residual magnesium is higher than the smallest concentration of supplemental magnesium test, 0.01 mM Mg^{2+}, so all the magnesium amounts are outside of the sensor's dynamic range.

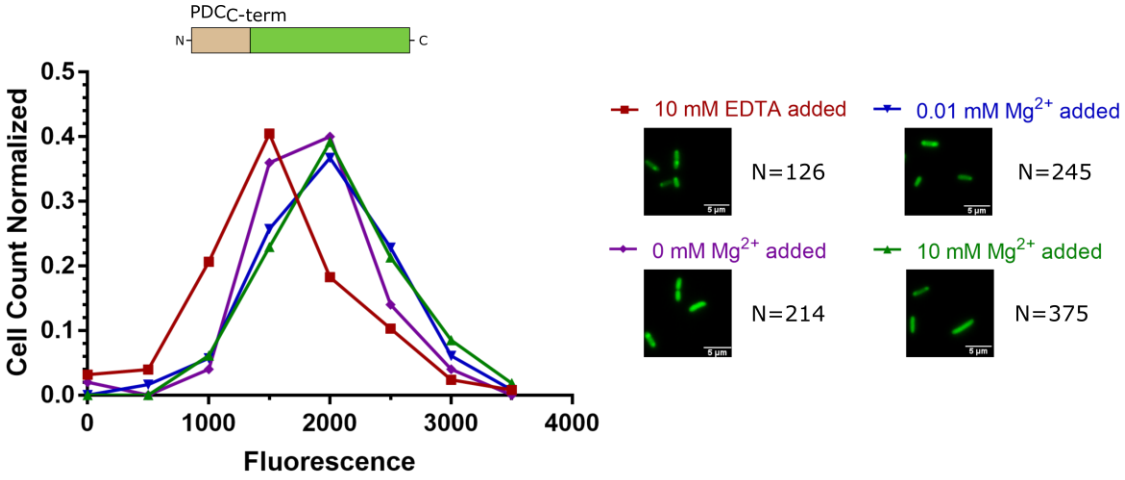

Figure 28: $PDC_{C\text{-}Term}$ Fusion Sensor fluorescence at various magnesium concentrations. Left) Wash assay with media swap graph with cartoon of sensor design inset. Right) Representative cells of the wash assay and the number of cells included in the analysis.

Between fluorescence values of 2500 to 3500, the $PDC_{C\text{-}Term}$ sensor displayed an increase of cells with fluorescence in this range upon addition of magnesium

sulfate. However, I did not observe dose-dependent changes in signal. Further analysis of lower magnesium is needed to determine if there is a gradual magnesium dose-dependent change in fluorescence. Currently, I do not know if 0.01 mM and 10 mM have the same effect on the PDC sensor. The run with no extra magnesium added still has magnesium stored by the cell, which can activate the sensor. Optimization of the washes with EDTA in the assay as well as more magnesium concentrations is needed to further test the responsive of this construct. Moreover, while small changes in fluorescence were observed, the degree of fluorescence change was not sufficiently robust to serve as a biosensor to interrogate host-microbe interactions via microscopy. Subtle changes in the fluorescence signal may indicate that further insertions near the PDC C-terminus could further improve the sensor responsiveness.

I tested the functionality of the $PDC_{N\text{-}Term}$ fusion sensor, where the C- terminus of cpGFP was fused to the N- terminus of the PDC domain (Figure 29). The $PDC_{N\text{-}Term}$ fusion sensor presented the most amount of fluorescence when it was treated with EDTA. Testing cpGFP and GFP fluorescence against the effects of EDTA addition will allow me to determine if this effect is from the lack of available magnesium near the chromophore to stabilize the sensor. The average total cell fluorescence intensity minus the average intensity of BL21 values for 0 mM magnesium sulfate, 0.01 mM magnesium sulfate and 10 mM magnesium sulfate, and 10 mM EDTA supplemented M9 are 2009 ± 839, 1950 ± 669, 1761 ± 715, and 2379 ± 829 respectively. An ANOVA test was performed between each magnesium concentration at a 95% confidence interval. There is no significance of the variation in magnesium sulfate on the fluorescence of this sensor.

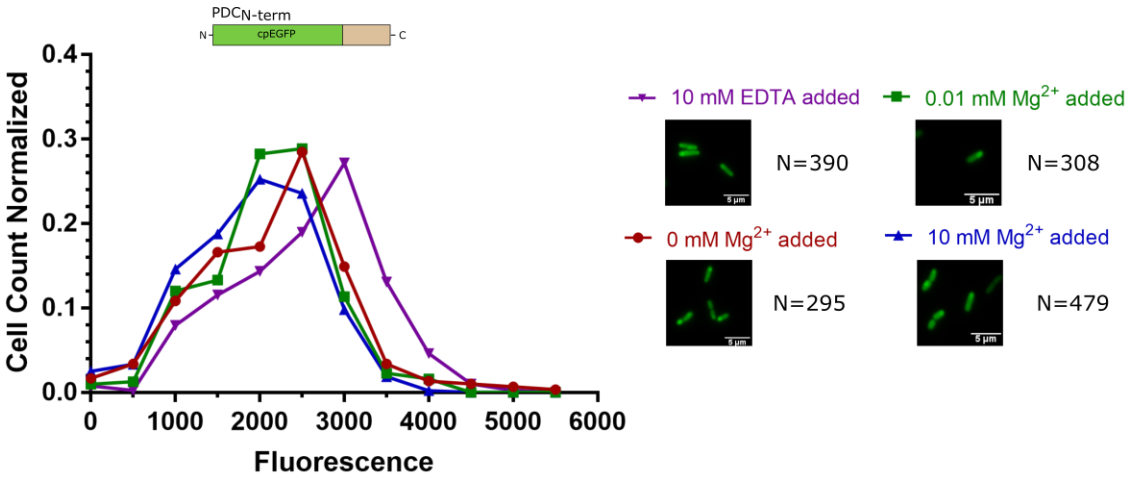

Figure 29: $PDC_{N\text{-}Term}$ Fusion Sensor fluorescence at various magnesium concentrations. Left) Wash assay with media swap graph with cartoon of sensor design inset. Right) Representative cells of the wash assay and the number of cells included in the analysis.

Based on the initial data shown above, the $PDC_{N\text{-}Term}$ fusion sensor did not display magnesium-dependent changes in fluorescence, suggesting that this fusion site may have either impacted magnesium binding or is in a region that does not undergo significant conformational change. This could be due to the insertion site; the terminal helix conformational change during the scissoring motion upon magnesium binding might not alter the environment near the cpGFP chromophore. As a follow up, the linker connecting the PDC domain and cpGFP could be hindering the necessary interactions. Optimization of the linker to impact the chromophore is described in the alternative strategies section below.

I next tested the functionality of the PDC_{115} fusion sensor, where cpGFP was inserted into the PDC domain at amino acid 115 (Figure 30). The PDC_{115} fusion sensor presented no significant change in fluorescence upon addition of magnesium sulfate. The average total cell fluorescence intensity for the sensor was 0.7- 1.8-fold over the autofluorescence of BL21 cells (Figure 49), indicating that expression levels of this

construct are low or that the protein is in a non-fluorescent conformational state. An ANOVA test was performed between each magnesium sulfate concentration at a 95% confidence interval was performed and indicated there is no significance of the variation in magnesium sulfate on the fluorescence of this sensor.

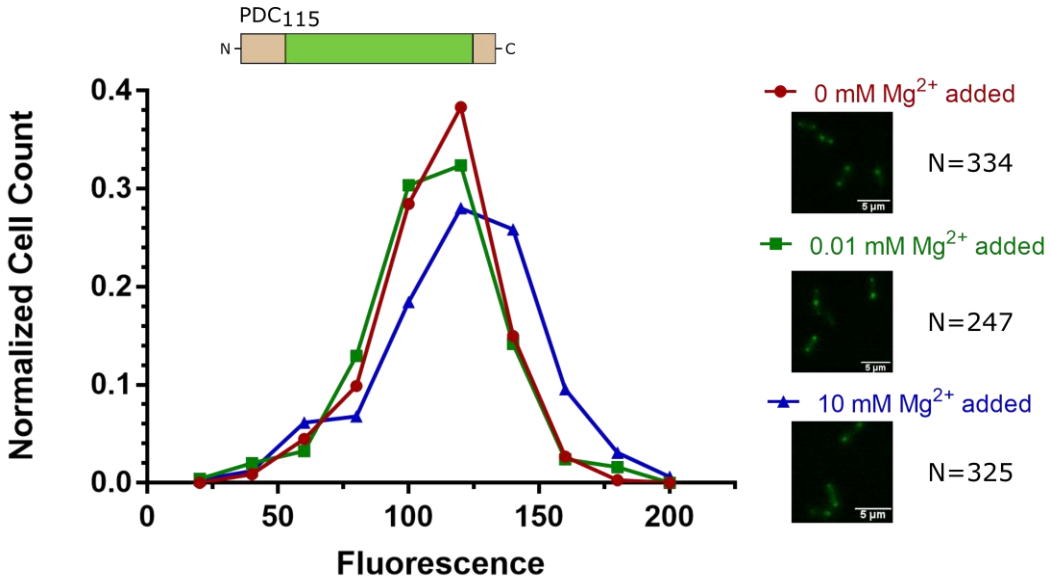

Figure 30: PDC_{115} Fusion fluorescence at various magnesium concentrations. Left) Wash assay with media swap graph with cartoon of sensor design inset. Right) Representative cells of the wash assay and the number of cells included in the analysis.

PDC_{115} fusion sensor design had 10-fold less fluorescence than the terminal fusion sensors and eGFP. There is a greater accumulation of fluorescence in foci compared to previous designs, indicating the protein has potentially misfolded into an inclusion body. This reduction in fluorescence could be due to: non-fluorescent protein conformation, misfolded protein aggregates, or low protein expression. Therefore, my first steps in troubleshooting this design is to confirm protein expression levels by western blot using the Anti-GFP antibody.

I tested the functionality of the PDC_{55} fusion sensor where cpGFP was inserted into the PDC domain at amino acid 55 (Figure 31). The PDC_{55} fusion sensor presented no significant change in fluorescence as more magnesium was added. An ANOVA test was performed and it indicated there is no significance of the variation in magnesium on the fluorescence of this sensor.

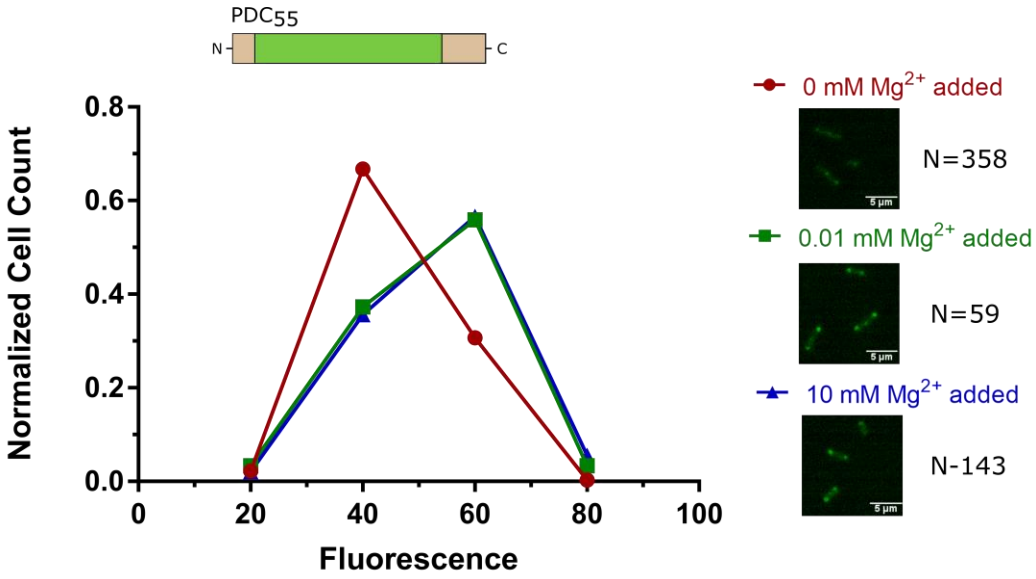

Figure 31: PDC_{55} Fusion fluorescence at various magnesium concentrations. Left) Wash assay with media swap graph with cartoon of sensor design inset. Right) Representative cells of the wash assay and the number of cells included in the analysis.

This design also had less fluorescence than the autofluorescence of Bl21 cells (Figure 49). There is also an accumulation of the little fluorescence into observed foci, which likely represented a misfolded inclusion body. Therefore, I suspect that the fusion site may have made the protein fold unstable during protein folding. Alternatively, this may also be due to poor expression of the PDC55 sensor, therefore I aim to further investigate expression via western blot analysis.

Based on the above analysis, immediate steps to determine functionality *in vivo* includes troubleshooting expression of the sensors and confirming equivalent levels of expression of each sensor during the wash assay. It is important to test a tighter range within 0-10 μM of supplemented magnesium to determine the lowest concentration the sensors will respond to.

Assessment of wash assay

To evaluate the effectiveness of my wash assays, I attempted to demonstrate the GCaMP6f[73] fluorescence dependence on calcium to prove my wash technique is adequate to introduce the small ions into the cytoplasm (Figure 32) The GCaMP6f sensor was previously used by the Kralj lab for single cell analysis in *E. coli*,[73] where they saw a 2-fold response in fluorescence with the addition of 5mM calcium to their imaging pad during the microscopy time-lapse. Addition of 10 mM EGTA to the pad caused a 0.5-fold decrease in fluorescence. Multiple small increases (1.2 fold) in fluorescence were also observed when imaging a single cell over 200 second time frame. I used the same methods as with supplemented magnesium M9, expect with supplemented 1 mM, 5 mM or 10 mM $CaCl_2$. I then imaged the cells on a pad composed of the same calcium chloride concentration.

I performed an ANOVA test between each calcium chloride concentration at a 95% confidence interval. The P value for this assay was >0.9999, confirming there is no significance of the variation in calcium addition on the fluorescence of GCaMP6f. A trial without the addition of calcium and a trial with the addition of EGTA (a known Ca^{2+} chelator) will be used to further investigate this previously published cpGFP calcium sensor. The autofluorescence of BL21 (Figure 49) was 1.5-fold over the

fluorescence of the fluorescence of GCaMP6f, providing evidence that expression levels of this construct may be very low. Since only one replicate was collected and there is no baseline (no external calcium added), more studies are needed to investigate this control sample. These studies will also be coupled with western blot analysis to confirm expression of the sensors,

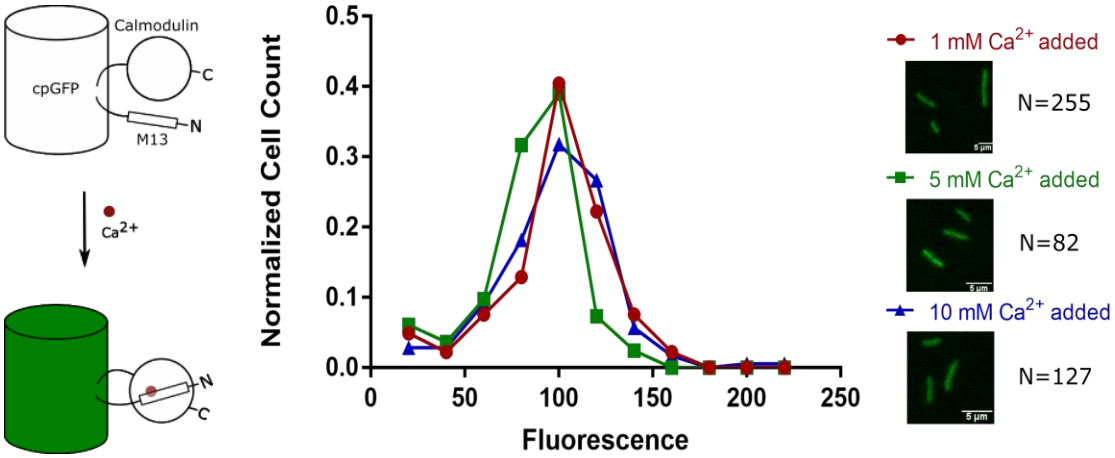

Figure 32: GaCMP6f fluorescence at various magnesium concentrations. Left) The conformational change of M13 binding to calmodulin upon the binding of calcium will cause cpGFP to fluoresce. Middle) Wash assay with media swap graph. Right) Representative cells of the wash assay and the number of cells included in the analysis.

To trouble shoot the GCaMP6f sensor as my assay control, I can run the time-lapse assay of the sensor expressed in media with no calcium. I can test if adding extracellular calcium in the imaging pad will cause spikes in fluorescence over time in a single cell because the kinetics are fast. The exponential decay occurs after 400 ms and the return to peak fluorescence time of 80 ms.[74]

Assessment of rationally designed sensors' functionality in vitro

The sensors were also tested for sensing capability through an *in vitro* fluorescence assay. Sensors were expressed and purified in buffer without additional magnesium sulfate. In a dark 96 well plate, protein was titrated with increasing

magnesium concentrations. Two sensors and eGFP control were purified at the time of this document. Because of low quantities of purified protein, only one trial was run at each magnesium sulfate concentration. The other four sensors, cpGFP control and repetitive trials will also be assayed in this manner.

The standard curve of eGFP shows increase in fluorescence as the protein concentration increases, in a linear mode. The titration of magnesium has no effect on the fluorescence of eGFP (Figure 33).

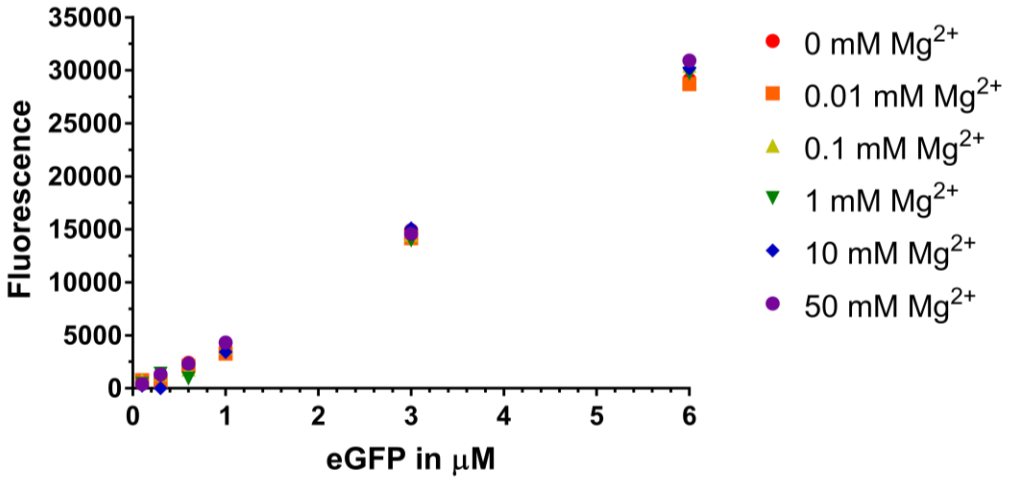

Figure 33: Fluorescence assay of eGFP against various magnesium concentrations. The titration of increasing magnesium does not affect the fluorescence of eGFP *in vitro*.

$PDC_{C\text{-}term}$ fusion and PDC_{Nterm} fusion Sensors had an increase of fluorescence as concentration of protein increased, except for at 3 μM concentration of protein (Figure 37), as the EGFP control did. With replicates of these trials, the fluorescence of 3 μM can be reevaluated for error.

At 0.1 μM of protein, the purified $PDC_{C\text{-}term}$ and $PDC_{N\text{-}term}$ sensors had 13-fold to 50-fold more fluorescence than purified eGFP (Figure 34). This 13-50- fold difference in fluorescence may indicate that significant amounts of the eGFP control

protein are misfolded. Therefore, in the future I aim to analyze each fluorescent protein construct using gel filtration and circular dichroism. The $PDC_{C\text{-}term}$ and $PDC_{N\text{-}term}$ sensors had a less than a 1-fold change of 0.01 mM supplemented magnesium sulfate over no supplemented magnesium sulfate. If there was a functional sensor, the magnesium sulfate would switch the sensor into the opposite state as no additional magnesium sulfate. There is an visual trend for $PDC_{N\text{-}term}$ sensor: as the magnesium concentration increases, the fluorescence decreases. Future replicates will allow determination if $PDC_{N\text{-}term}$ sensor turns off in the presence of magnesium. This fold change could be the baseline fluorescence of cpGFP. These controls will determine if high fluorescence of the sensor is constitutive fluorescence or magnesium dependence activity.

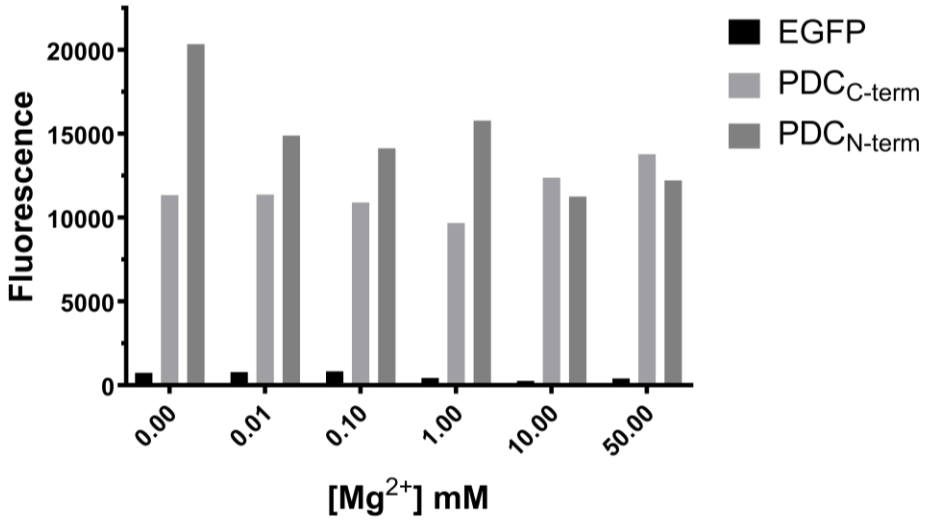

Figure 34: Fluorescence assay of 0.1 μM of purified eGFP, $PDC_{C\text{-}term}$ fusion sensor, and $PDC_{N\text{-}term}$ fusion sensor against various magnesium concentrations. The titration of increasing magnesium does not affect the fluorescence of eGFP *in vitro*.

At 0.3 μM of protein, the purified $PDC_{N\text{-}term}$ fusion sensor in 0.01 mM magnesium sulfate supplemented media had the same fluorescence than the sensors

in 0 mM supplemented media (Figure 35). If the $PDC_{N\text{-}term}$ fusion was a functional sensor, the fluorescence would increase as the supplemented magnesium increased. There is an opposite trend, again, for $PDC_{N\text{-}term}$ sensor: as the magnesium concentration increases, the fluorescence decreases. This is consistent with the trials run at 0.1 μM of the purified sensor. Replicates of these trials will allow determination if $PDC_{N\text{-}term}$ sensor turns off in the presence of magnesium. Analyzing the fluorescence of cpGFP in this manor will allow conclusions on the large increase of fluorescence over EGFP. This fold change could be the baseline fluorescence of cpGFP. These controls will determine if high fluorescence of the sensor is constitutive fluorescence or magnesium dependence activity.

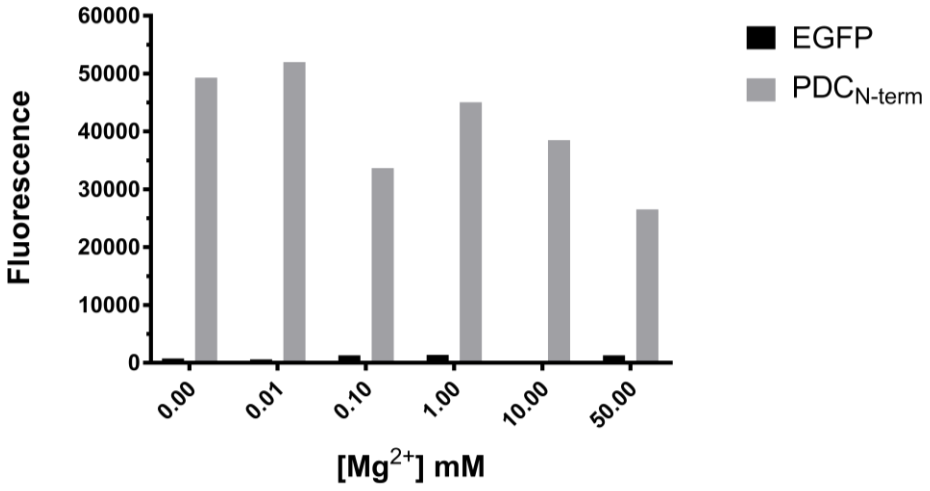

Figure 35: Fluorescence assay of 0.3 μM of purified eGFP and $PDC_{N\text{-}term}$ fusion sensor against various magnesium concentrations. The titration of increasing magnesium does not affect the fluorescence of eGFP *in vitro*.

At 0.6 μM of protein, the purified $PDC_{C\text{-}term}$ exhibited a 3-fold increase upon addition of 0.01 mM magnesium sulfate over 0 mM magnesium sulfate (Figure 36), providing a line of evidence that $PDC_{C\text{-}term}$ is a functional magnesium sensor. However, at concentrations higher than 0.01 mM MgSO4, the fluorescence of the

sensor is no longer increases, potentially due to binding site saturation. Replicates of these trials, closely examining magnesium sulfate concentrations between 0 and 0.01 are needed to demonstrate the sensor's fluorescence is dependent upon binding magnesium. Moreover, analyzing the fluorescence of cpGFP is necessary as a baseline control.

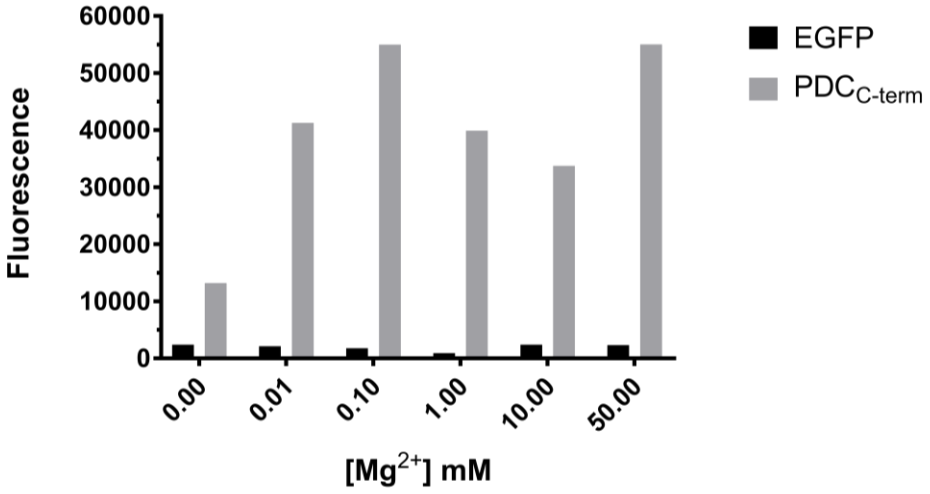

Figure 36: Fluorescence assay of 0.6 μM of purified eGFP and PDC$_{C\text{-term}}$ fusion sensor against various magnesium concentrations. The titration of increasing magnesium does not affect the fluorescence of eGFP *in vitro*.

At 3 μM of protein, the purified PDC$_{N\text{-term}}$ fusion sensor and PDC$_{N\text{-term}}$ fusion sensors in supplemented magnesium sulfate media had similar fluorescence to 0 mM supplemented magnesium sulfate (Figure 37). These fluorescence values seemed out of place because the fluorescence values are lower than other protein concentrations sampled (Figure 34, Figure 35 and Figure 36), although I would expect the sensors to have similar fluorescence to the positive control of EGFP. If there was a functional sensor, the fluorescence would increase as the supplemented magnesium increased. There is a visual trend of PDC$_{C\text{-term}}$ sensor turning on in the presence of more

magnesium. Replicates of these trials will allow determination if this is a true dose dependent curve. Analyzing the fluorescence of cpGFP is necessary to determine the baseline fluorescence of cpGFP. These controls will determine if high fluorescence of the sensor is constitutively fluorescent or if magnesium-dependence is present.

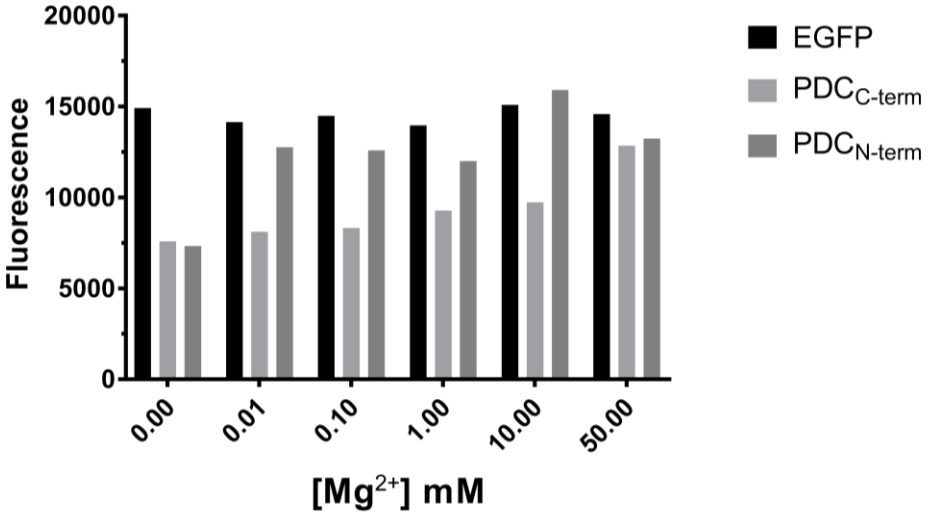

Figure 37: Fluorescence assay of 3μM of eGFP, $PDC_{N\text{-}term}$ fusion sensor, and $PDC_{C\text{-}term}$ fusion sensor against various magnesium concentrations. The titration of increasing magnesium does not affect the fluorescence of eGFP *in vitro*.

Analyzing the functionality of the sensors *in vitro* assisted in evaluating the concentrations of supplemented magnesium sulfate chosen. I will proceed by testing concentrations with in the 0-0.01 mM supplemented magnesium sulfate to achieve a magnesium-dose dependent curve of fluorescence. I also will continue replicating trials of the sensors shown here, as well as assaying purified cpGFP and sensors PDC_{55} and PDC_{115} against magnesium sulfate. Because the PhoQ PDC domain is also sensitive to calcium ions, I will test the effectiveness of the sensor designs against varied calcium concentrations.[45]

To begin the domain insertion library approach, I have designed the staging plasmid (Figure 25) with the HIS tag labeled PDC domain flanked by BsmbI Type IIS restriction enzyme cut sites on a plasmid vector with a T7 promoter. I will design a plasmid with the Mu transposon containing an antibiotic gene[69] flanked by the BsaI Type IIS restriction enzyme cut sites and a plasmid with cpGFP flanked by the BsaI Type IIS restriction enzyme cut sites; primers will be designed to amplify the mu transposon and cpGFP inserts. The expression vector I will use is an *araC* promoter, the same expression vector I have used for *in vivo* assays. Next, I will follow the protocol outlined in the DIP-seq methods paper.[69]

Alternative strategies to design a cpGFP sensor for the PhoQ magnesium sensing signaling pathway

The first generation of these designs, sensors $PDC_{C\text{-}Term}$ Fusion and $PDC_{N\text{-}Term}$ Fusion, do not include the TM-helices, while the second generation will include part of the helices as the linker between cpGFP and PDC fusion, as I predict the scissoring motion could cause the greater conformational and environmental change needed to stabilize the cpGFP chromophore.

Second generation sensors will focus on the linkers connecting the ligand-binding domain and cpGFP. In the design of GCaMP2, the N terminus and C terminus of cpGFP each have a two amino acid linker, LE and TR, respectively. This linker has been shown to be impactful on the fluorescence of the cpGFP sensitivity to calcium in GaCMP.[57] If the amino acids are basic, the sensor no longer responds to calcium or if the amino acid has a hydroxyl group, the cpGFP will undergo photoisomerization.[57]

Another consideration about the assay design is the ability of the PhoQ PDC domain to acutely sense small changes in magnesium concentration in the cytosol. I

have added an N-terminus export tag to the sensors, peptide TorA. This tag allows GFP to fully fold and mature in the cytoplasm before exportation to the periplasm.[75] With this tag, I can see if the sensors are more sensitive to supplemental magnesium concentrations compared to the cytosolic concentration of magnesium.

Without further *in vitro* and *in vivo* experiments, we cannot identify a strong candidate as a rational design cpGFP biosensor. Four sensors have yet to be evaluated via *in vitro* fluorescence assay and two have yet to be images *in vivo.* We propose to move the rational design library shown in these results into a domain insertion profiling library discussed in Figure 24.

Dimerization-dependent Fluorescent Proteins as Biosensors

In 2012, the Campbell Lab engineered the tetrameric red fluorescent protein to create a dimerization-dependent fluorescent protein.[2] The goal was to create a dimly fluorescent monomer (monomer A), whose fluorescence was rescued by the dimerization of a compatible monomer (monomer B).

To achieve a monomer of RFP, a well-established protocol was used to make two mutations (H162K and A164R) on the dimerization interface of one monomer of the dTomato dimers. This engineered monomer is called Monomer A. Two library screening methods were used to find a Monomer B to rescue dimer formation and fluorescence: an electrophoretic mobility shift screen for heterodimeric pairs of RFPs and a replica-plating screen for fluorogenic and heterodimeric pairs of RFPs.

Analysis of the final versions of monomers A and B was done through homology modeling to understand the mutations made through the library screenings. Two nonconservative mutations, S146A and K163G, in monomer A destabilize the chromophore by eliminating a hydrogen bond and electrostatic interactions. Four nonconservative mutations, K70E, Y120C, I161S, and E215G in monomer B prohibits the formation of the chromophore. Between monomers A and B, there are 15 mutated-residues on the dimerization face of the β barrels. The key alanine to an arginine (A164R) mutation, prevents monomers of A from self-dimerizing by steric charge repulsion between positively charged arginines. The dimerization of monomers A and B was rescued by two mutations on monomer B that

created a "hole", across from the A164R mutation on monomer A, creating "bump-and-hole" interactions during the dimerization of A and B.[2]

The dimerization of the monomers has 10-fold brighter fluorescence state than the dissociated monomer A, creating intensometric sensors with reversible fluorescence response. The red dimerized fluorescent proteins have a K_d of 33 μM, therefore, the monomers exist in the dissociated state in eukaryotic cytoplasmic concentrations.[2] These properties of the dimerization-dependent fluorescent proteins are unique compared to the current fluorescent protein sensor tool box, however they each come with disadvantages. As mentioned above, the chromophore stabilization is sensitive to pH, which may affect where the sensors can be used with in the cell. With the impressive 10-fold brighter fluorescence between dissociated and dimerized states, the fact that monomer A retains 10% fluorescence of the dimerized constructs may lead to convoluted data if used in a high throughput screen. The sensors are best used as a monochromatic alternative to FRET sensors, in elucidating protein-protein interactions that involve dimerization of native proteins. These red hue dimerization dependent sensors.

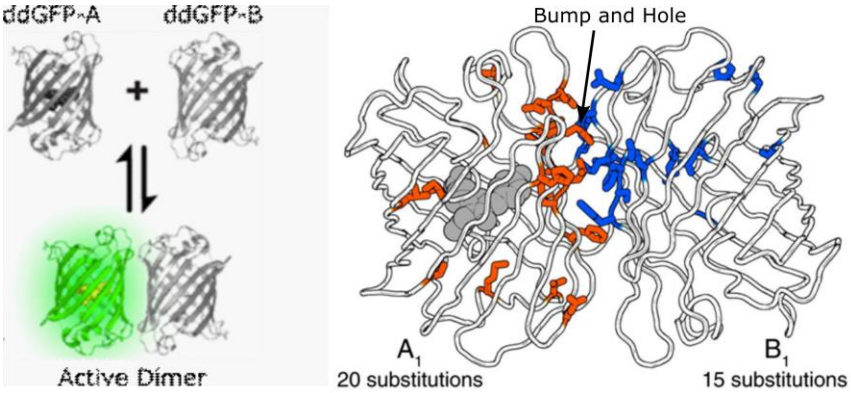

Figure 38: Heterodimerization Dependent Fluorescence. Left panel) Scheme of the ddGF proteins functionality. Right panel) Homology model of heterodimers ddRFP A and B. The mutations on the dimerization face, including

the 'bump and hole" residues, create heterodimerization and fluorescence. The mutations facing into the beta barrel of ddRFP A reduce the stability of the chromophore. The mutations facing into the beta barrel of ddRFP B remove the ability of chromophore formation.[2] Panal A is reprinted with permission from "Dimerization-Dependent Green and Yellow Fluorescent Proteins." Spencer C. Alford, Yidan Ding, Thomas Simmen, and Robert E. Campbell; ACS Synthetic Biology 2012 1 (12), 569-575. *Copyright 2012 American Chemical Society.* [76] Panel B is from Alford *et* al. Copyright © *2012 Elsevier Ltd. All rights reserved.*

Later in 2012, the Campbell Lab engineered the red dimerization-dependent fluorescent protein (ddFP) monomers to create green and yellow dimerization-dependent fluorescent proteins. These mutations in ddRFP monomer A include A71M and V105A for green fluorescence and M66C for yellow fluoresnce, which have been previously shown to alter chromophore properties.[77, 78] The monomers ddGFP A and ddYFP A were then screened by error-prone mutagenesis library and by fluorescence to establish copies with high green or yellow fluorescence and low red fluorescence.[79] The green and yellow variants have high affinity between monomers, with K_d of 9 μM and 14.5 μM respectively.[76] These affinities are increased from the parent pair ddRFP-AB, K_d of 33 μM.[2] Because of the high affinity between monomers, the Campbell Lab decided the green ddFP pair are suitable for tethered protein studies: protein localization and proximity events such as membrane-bound protein and cytosolic protein interactions at cell membrane.

The green ddFPs were fused to membrane localized proteins in a proof of principle experiment to fluorescently label the Mitochondria- Endoplasmic Reticulum endomembrane contact sites (MAM). Calnexin (CalN), an ER endomembrane chaperone protein, was fused to green ddFP-A; protein translocase of outer membrane-20 (Tom20), a receptor on the outer membrane of the mitochondria, was fused to green ddFP-B. The chimeras were designed to allow the ddFP monomers to be cytosolic (Figure 39). The CalN-ddFP-A and Tom20-ddFP-B were co-expressed

with mCherry that is either localized to the mitochondria or to the ER membrane. The green ddFP pair labeled the MAM with green fluorescence, and colocalized with the red fluorescence that labeled the mitochondria (top row) and the ER (bottom row) (Figure 39).

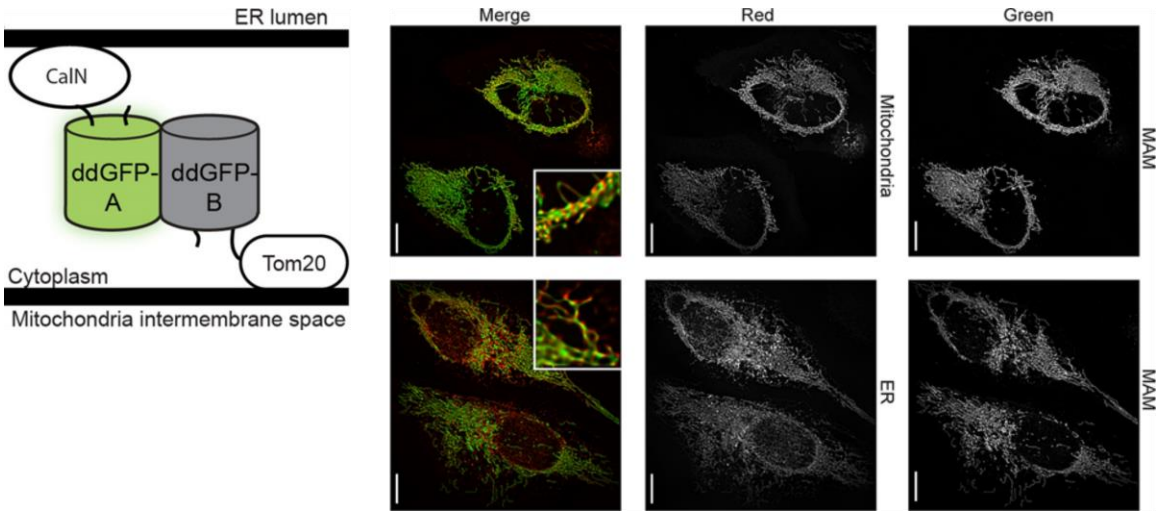

Figure 39: Left panel) ddGFP labeling of two proteins, CalN and Tom20, known to localize to the space between the ER and the mitochondria (MAM). Right panel) microscopy images of mammalian cells. The merge column indicates there is colocalization of the red fluorescence (mitochondria or ER labeling) and the green fluorescence (MAM labeling). Reprinted with permission from "Dimerization-Dependent Green and Yellow Fluorescent Proteins." Spencer C. Alford, Yidan Ding, Thomas Simmen, and Robert E. Campbell; ACS Synthetic Biology 2012 1 (12), 569-575. *Copyright 2012 American Chemical Society.* [76]

Because of the high affinity between the green monomers, the sensors do not lend to free dissociating sensor strategies, like the red dimerization dependent fluorescent proteins. The high affinity of the ddGFP pairs would limit the ability to control for ddFP dimerization driven events or for diffuse protein-protein interactions. However, the green dimeric state is 60-fold brighter than the dissociated state. In tethered studies, the dimerization-dependent fluorescent proteins will aid in cellular processes studies with single-FP design and high contrast. Further

optimization of affinity of the heterodimers will expand the applicable studies: such as transient protein-protein interactions.

Even though the Campbell lab optimized the ddFP B copy to enhance the fluorescence of the ddFP A copy for all three colors, they discovered that the ddFP B copy was interchangeable between red and green ddFP A copies.[46] They designed Fluorescent Protein Exchange biosensors that relied on the ratio-metric fluorescence color changes that occurs when the ddFP B copy exchanges ddFP A binding partners due to protein-protein interaction control. They tested the Fluorescent Protein Exchange technology with Ca^{2+} -mediated protein-protein interactions between calmodulin (CaM) and peptide M13 (Figure 40). The increases in the red correlated with the histamine-stimulated Ca^{2+} oscillations. The increases of red fluorescence correspond to the association of CaM and M13, promoting red ddFP A association with ddFP B.

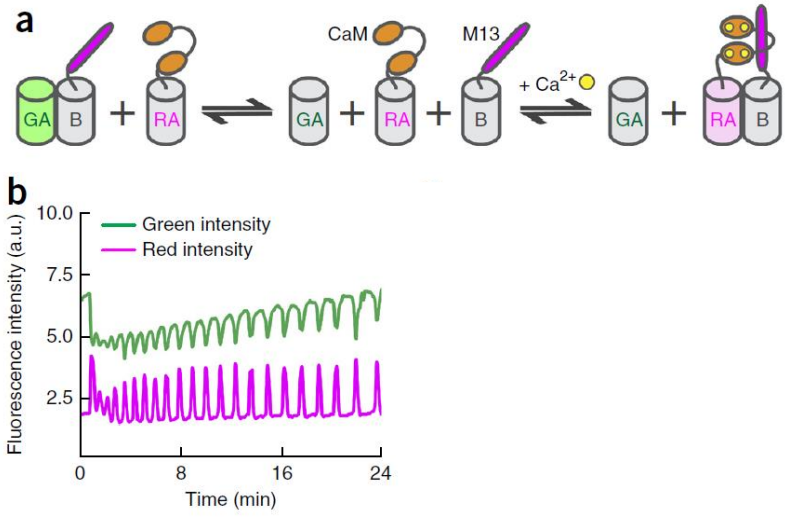

Figure 40: Fluorescent Protein Exchange Sensor. A) Calcium sensor design using the Fluorescent Protein Exchange dimerization dependent fluorescent proteins to signal when the Calcium-mediated interaction of CaM and M13 occur. B) Red and green fluorescence intensity over time of a HeLa cell stimulated for calcium oscillations. Figure from Ding *et al. Copyright © 2015, Springer Nature*[46]

Next, the Campbell lab tested the Fluorescent Protein Exchange technology as a single intermolecular-protein biosensor to simplify the transfection to one plasmid and to normalize the cell-to-cell variability in expression, and therefore fluorescence, ratios. The schematic for this design is shown in Figure 41 A, the Fluorescent Protein Exchange single-protein biosensor chimera is red ddFP-A – CaM – ddFP-B – M13 – green ddFP-A. The ddFP-B copy can associate with both ddFP-A copies in equilibrium, until histamine-induced Ca^{2+} oscillations which will promote the association of CaM and M13. They observed an 4-fold increase in the red-to-green fluorescence color ratio upon histamine-induced Ca^{2+} oscillations (Figure 41).[46]

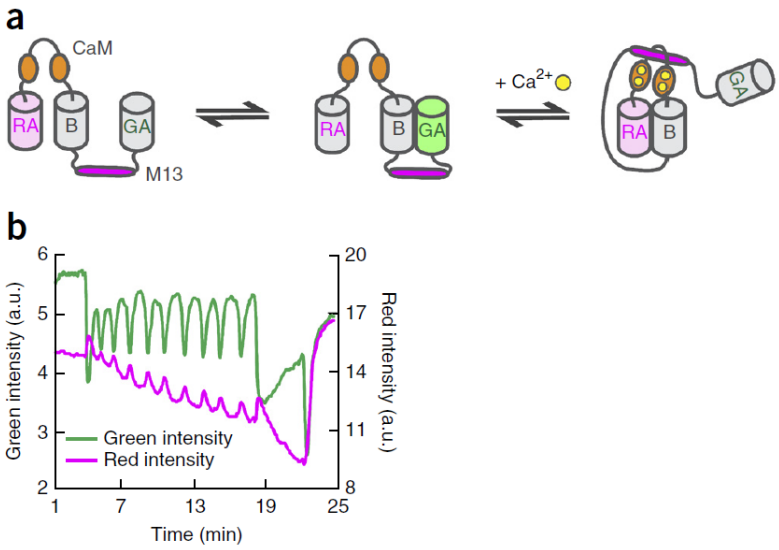

Figure 41: Single protein fluorescent protein exchange sense design. A) Single protein Fluorescent Protein Exchange sensor to signal when the Calcium-mediated interaction of CaM and M13 occur. B) Red and green fluorescence intensity over time of a HeLa cell stimulated for calcium oscillations. Figure from Ding *et al. Copyright © 2015, Springer Nature* [46]

These studies provided evidence that both intermolecular and intramolecular Fluorescent Protein Exchange biosensor designs produced working, ratio-metric sensors, without lengthy linker optimization needed for previously published dimerization sensors. However, the dimerization-dependent fluorescent protein

exchange biosensors are only suitable for qualitative imaging applications due to the differing affinities of the ddFP-A copies to the exchangeable ddFP-B copy. These biosensors are best utilized for applications where qualitative information is sufficient because of the minimal design qualifications needed to build the ratio-metric biosensors.[46]

Using Dimerization-dependent Fluorescent Proteins as a Read-out of Two Component System Activity

We sought to design biosensors utilizing the dimerization properties of ddGFP-AB. The phosphorelay of a two-component system ends at the receiver domain of a response regulator (P~RR).[80] Certain response regulators can dimerize with a stronger affinity when phosphorylated.[81] This pair of P~RR then acts as a transcription factor by binding to DNA through a effector domain.[80] The OmpR/PhoB subfamily of response regulators have been studied for phosphorylation effects on dimerization. The Stock lab tested 17 response regulators in this family for increased dimerization when phosphorylated with FRET.[81] 16 of these homodimer pairs had increased FRET ratio upon phosphorylation.[81]

Since response regulator dimerization is impacted by phosphorylation, I hypothesize that ddGFPs can be used as a biosensor readout of signaling pathways' activity. The ddGFP read-out design utilizes the native phosphorylation pathway of a TCS: can active histidine kinase will phosphorylate its cognate response regulator, which causes the response regulator to dimerize with another cognate phosphorylated response regulator. The ddGFPs will be attached to known response regulators (Figure 42). This approach requires the optimization of the linkers

connecting the RR-ddGFP each time a new TCS is tested. The first-generation design utilized the well characterized HK/RR system PhoQP (OmpR/PhoB subfamily RR). The histidine kinase PhoQ phosphorylates response regulator PhoP under low magnesium conditions. The phosphorylated PhoP proteins can dimerize and bind DNA as a transcription factor. The phosphorylation of receiver domain PhoP was proven to promote dimerization of the response regulators.[81]

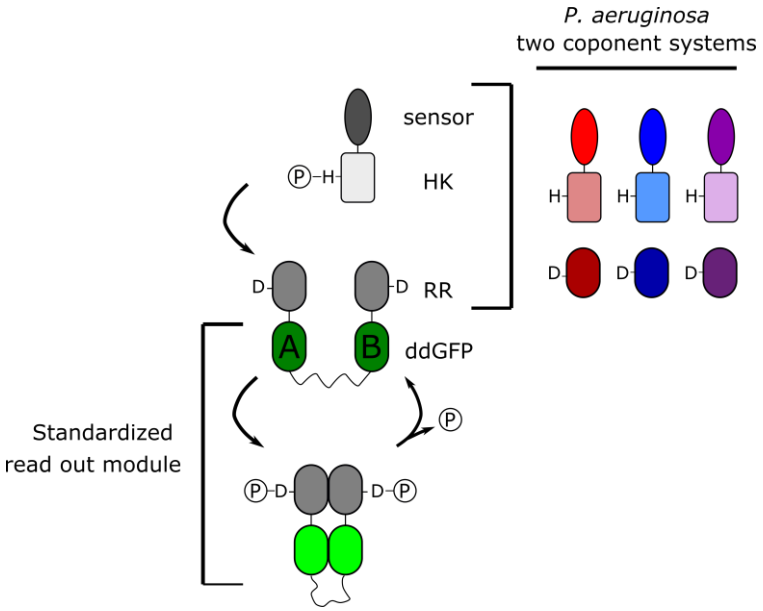

Figure 42: Dimerization-dependent Readout Models. In this approach, the HK and RR of a TCS will be tested by the modular read out of dimerization-dependent GFP fused to the RR.

Results and Proposed Studies

Samuel Duvall, a senior graduate student in the Childers, designed positive controls for the use of the ddGF proteins. He set out to determine the maximum fluorescence of the ddGF proteins by attaching leucine zippers to the termini of the ddGF proteins (Figure 44A). The combination of ddGFP A-LZ and LZ-ddGFP B gave the highest fluorescence in *Caulobacter crescentus*, a gram-negative bacterium

(Figure 43). There was minimal fluorescence of monomer A or monomer B expressed alone.

I designed a positive control where the ddGF proteins were connected by a flexible linker from C-terminus of ddGFP A to the N-terminus of ddGFP B; which allows the construct to adopt a conformation that brings the two proteins close together (Figure 44B). In the negative control, the ddGF proteins are connected by a rigid linker designed from fibernectin that links the C-terminus of ddGFP A to the N-terminus of ddGFP B, preventing the two proteins from encountering one another by preventing the conformational flexibility found in the positive control (Figure 44C). At low intracellular protein concentrations, we expect the flexible linker will allow the ddGF proteins to dimerize and fluoresce, but the rigid linker will keep the ddGF proteins apart, and limit fluorescence. I will determine quantitatively the responses of these controls by microscopy. ddGFP A and ddGFP B will also be expressed individually and together to collect information on background fluorescence of the individual fluorescent proteins in diffuse conditions.

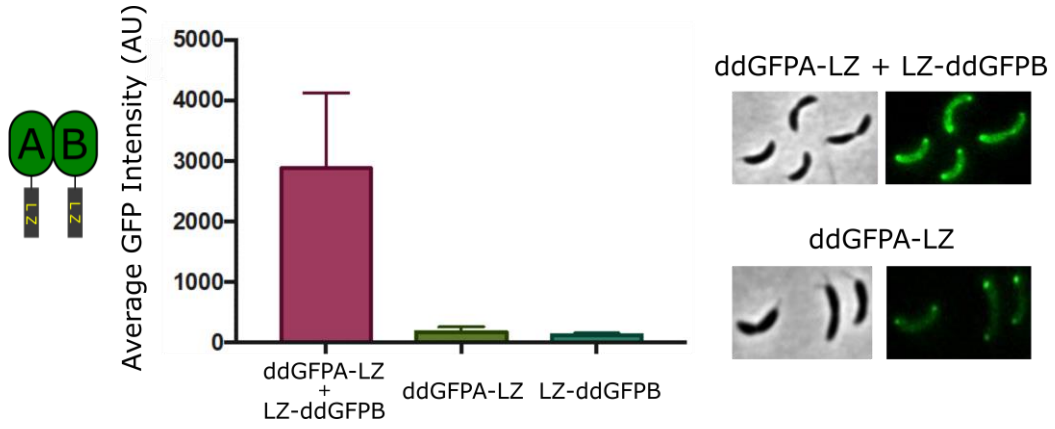

Figure 43: Average GFP intensity of the forced dimerization of monomer A and monomer B by leucine zippers in *C. cresentus*.

Design of a ddGFP sensor for the PhoQ magnesium sensing signaling pathway

I set out to design magnesium sensors with the TCS PhoQP. Based on the PDB model of dsRed dimers A and C (the structural basis for ddGFP dimers used by the Campbell lab)[2], I chose to fuse the response regulator domain of PhoP (PhoP-RR) to the N-terminus of ddGFPA and to the C-terminus of ddGFPB because of the proximity of the termini in the dimer structure, and both have a flexible secondary structure. There is a 16 residue flexible linker, between ddGFP and PhoP-RR, composed of two repeats of this sequence: GGSGSGSS (Figure 44). Because the sensor ddGFP-RR will have to compete with native PhoP for phosphorylation, the biosensors are going to be designed for expression in ΔPhoP *E. coli* strain.

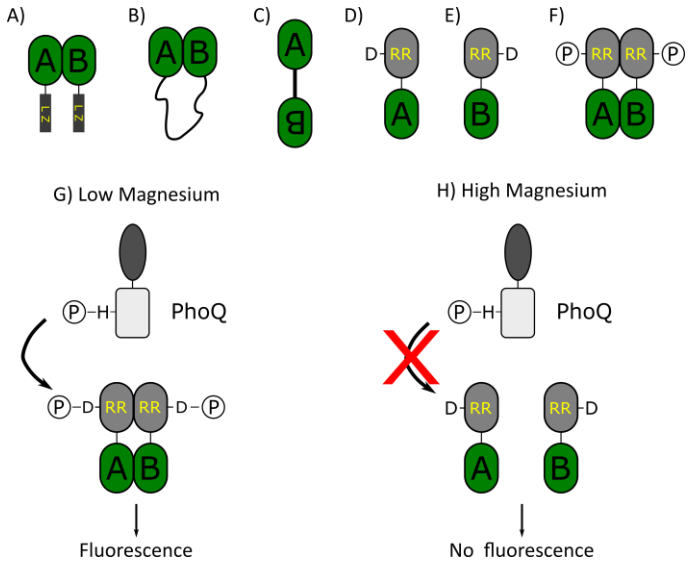

Figure 44: Cartoon depiction of controls and sensors. A) LZ are attached to each ddGFP monomer: ddGFPA-LZ and LZ-ddGFPB. B) ddGFP monomers A and B are connected by a flexible linker. C) ddGFP monomers A and B are connected by a rigid linker. D) ddGFP monomer A is connected to response regulator domain of PhoP: RR-ddGFPA. The phosphorylatable amino acid (Asp) is shown as the letter D. E) ddGFP monomer B is connected to response regulator domain of PhoP: RR-ddGFPB. The phosphorylatable amino acid (Asp) is shown. F) The dimerization of RR-ddGFPA and RR-ddGFPB is dependent on the phosphorylation of the RR. The phosphate group is shown as Ⓟ.

While attempting to test the designs of RR-ddGFPA, of RR-ddGFPB, and of the duel expression of RR-ddGFPA and RR-ddGFPB, in a ΔPhoP *E. coli* strain, I

encountered an expression problem relating to the plasmid vector I chose when cloning the sensor. The ΔPhoP *E. coli* strain does not have the T7 genes needed to express the T7 promoter. The araD gene is also deleted in the strain, causing a buildup of toxic intermediates of the arabinose metabolism pathway, therefor using an araC promoter would cause cell death. I need to optimize a constitutive promoter on a plasmid to us this ΔPhoP *E. coli* strain. This requires optimization of promoter strength and the necessary expressed protein concentrations. While I address the expression issue in the ΔPhoP *E. coli* strain, I chose to transform the sensors into BL21 to test the magnesium-sensing capabilities.

I hypothesized that cells expressing both RR-ddGFPA and RR-ddGFPB in the presence of low magnesium would result in a phosphorylated biosensor, triggering dimerization and high fluorescence in the cells (Figure 44G-H). Due to PhoQP endogenous responses to magnesium ions, high magnesium is predicted to result in unphosphorylated RR-ddGFPA/ddGFPB, and therefore dim fluorescence from monomeric sensors carrying copy A of the ddGFP. I expressed the sensors in M9 salts with either no magnesium, 0.01 mM magnesium, 2 mM magnesium, or 10 mM magnesium supplementation. These concentrations of magnesium were shown to influence PhoQP TCS: 0.01 mM magnesium confers with the ON state of PhoQP and 10 mM magnesium confers with the OFF state of PhoQP *in vivo*.[70] 2 mM magnesium is standard concentration for minimal media. Cells grown in no magnesium or 0.01 mM magnesium had slower growth rates and some cells had variation in phenotypes, such as elongation.

The *in vivo* assay of sensor RR-ddGFPA fusion protein expressed alone in M9 media supplemented with typical magnesium (2 mM) concentrations saw a 2.8-fold change over BL21 autofluorescence (Figure 45). An ANOVA test was performed between each magnesium concentration at a 95% confidence interval. The test indicated there is no significance of the variation in magnesium on the fluorescence of the monomer sensor.

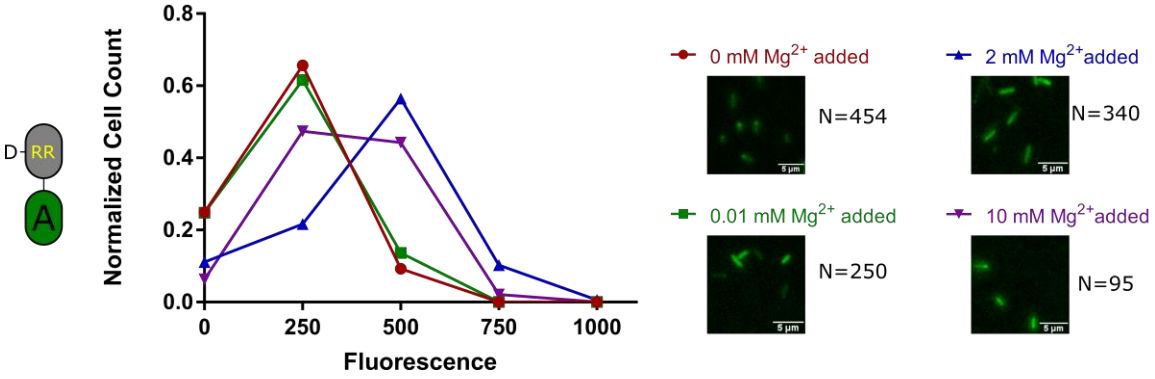

Figure 45: *in vivo* Fluorescence Imaging Assay of ddGFPA$_{\text{N-Term RR}}$ Fusion Sensor. The Y axis was normalized to one to account for the variation is cells counted for each experimental trial. The ddGFPA monomer is expected to have lower fluorescence, as the chromophore is mature. Addition of magnesium does not influence on the fluorescence.

The assay of sensor RR-ddGFPB fusion protein expressed alone in M9 supplemented with typical magnesium (2 mM) concentrations (Figure 46) saw a 2.5-fold change over background BL21 autofluorescence (Figure 49). ANOVA tests indicated there is no significance of the variation in magnesium on the fluorescence of the monomer sensor.

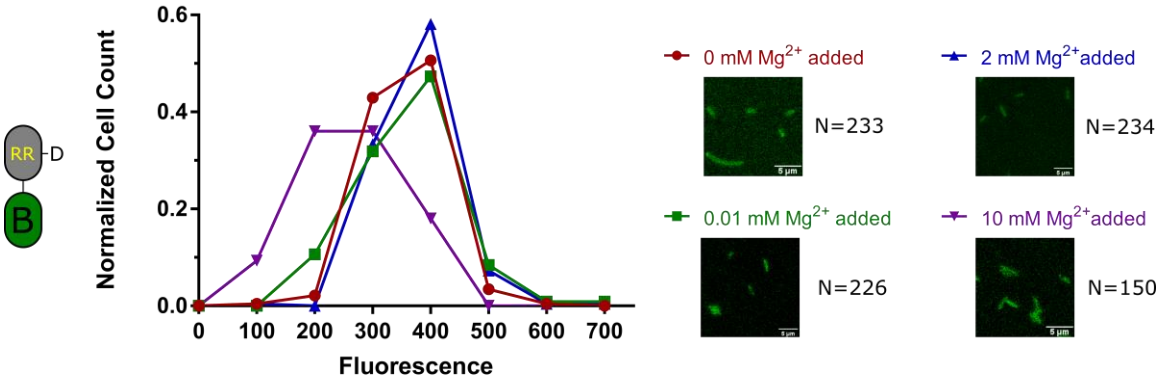

Figure 46: *in vivo* Fluorescence Imaging Assay of ddGFPB$_{\text{C-Term RR}}$ Fusion Sensor. The Y axis was normalized to one to account for the variation is cells counted for each experimental trial. The ddGFPB monomer should not show fluorescence, because the chromophore was mutated out. Addition of magnesium does not influence the fluorescence.

I would expect there to be a greater difference between the two sensors, as RR-ddGFPB does not have a mature chromophore to fluoresce. A western blot would confirm there is expression of each protein. By imaging cells expressing a GFP with the key catalytic glycine residue mutated to an alanine, I can compare the fluorescence of the dark GFP to the fluorescence of monomer B. Only one replicate was collected for assays; the high fluorescence of the sensor with monomeric B maybe an outlier.

When both the RR-ddGFPA and RR-ddGFPB sensors were expressed together on the same vector, two distinct populations can be seen for each experimental condition. The first population with a fluorescence intensity between 0 and 500 AU could correspond to the fluorescence of the monomer forms of RR-ddGFPA and RR-ddGFPB. A western blot would confirm there is similar expression of each monomeric sensor. The second peak at a higher average fluorescence could correspond to the dimerization of the two monomers to form the stabilized chromophore in monomer RR-ddGFPA (Figure 47). The addition of magnesium does not drive a decrease of

fluorescence according to an ANOVA test. However, I have only completed one replicate of this assay, more replicates will be collected to verify trends seen on the graph.

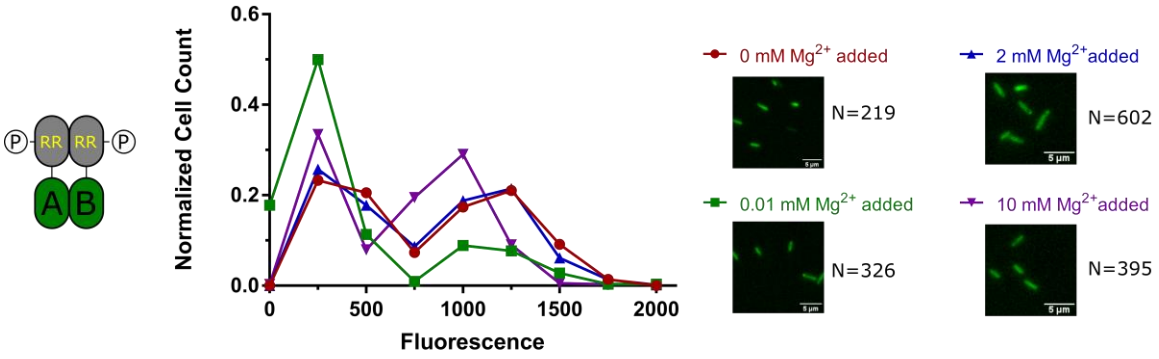

Figure 47: *in vivo* Fluorescence Imaging Assay of the duel expression of ddGFPA$_{\text{N-Term RR}}$ Fusion Sensor and ddGFPB$_{\text{C-Term RR}}$ Fusion Sensor. The Y axis was normalized to one to account for the variation is cells counted for each experimental trial. The first peak between 0 to 500 AU could correspond to the fluorescence of the sensor with monomer ddGFPA. The second peak between 1000 and 1500 AU could correspond to the dimerization of the two monomers ddGFPA/B. Addition of magnesium does not influence the fluorescence.

By visualization, the increase of supplemented magnesium from 0.01 mM, to 2 mM, to 10 mM causes a gradual increase in cell count at 1000 AU. The 0 mM magnesium trace could be a false positive. Adding supplemented EDTA to M9 media will determine the effect of no magnesium on the sensor's activity. Currently, the visual trend indicates in high magnesium the sensors are dimerizing. Increasing magnesium may influence the dimerization of monomers A and B. Assaying the diffuse monomers against a magnesium concentration titration will rule out an effect of magnesium on ddGFPA/B dimerization.

An alternative interpretation is that 10mM of magnesium triggers the phosphatase activity of PhoQ resulting in dephosphorylation of PhoP and monomerization of the sensor. To test this effect, smaller increments of magnesium

concentrations need to be used: the change in activity of the sensor could occur between 2 mM and 10 mM of magnesium, for example. Future experiments will conclude if there is a dose-dependent range of magnesium where the sensors are responsive toward.

After reviewing the original papers published on the dimerization depended proteins, I have discovered the K_D rate of the dimerization of the fluorescent monomers is similar to the response regulators in *E. coli in vitro*. This may prevent the dimerization of the RR-ddGFP sensors to be driven solely by the phosphorylated-RR dimerization, causing discrepancies of whether the sensor is responding to the input-signal of the TCS or close proximity to the partner monomer.

Additionally, I have designed TorA response regulator sensors because of the high specificity for homodimerization and the high FRET ratio of the dimerization of the phosphorylated RRs.[81] To confirm that this candidate exhibits a high binding affinity, I initially plan to purify and quantify the dimerization capabilities of TorA in its unphosphorylated versus phosphorylated states. Upon successful characterization of the TorA sensor, a chimeric HK can be constructed by replacing the TorA HK sensory domain with sensory domains from histidine kinases implicated in biofilm formation (Figure 48).

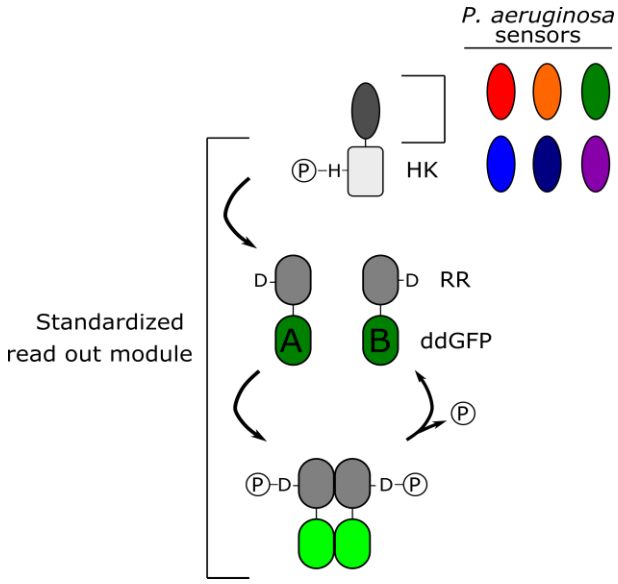

Figure 48: Dimerization dependent fluorescent readout. The standardized RR-ddGFP module will dimerize only by the phosphorylation of the RR by the HK. In this model, the fusion between the sensor and the orthogonal HK will be optimized for each sensor tested.

Experimental Procedures

Plasmid construction and strain preparation

Plasmid constructs were designed using J5 Vector Editor. From the J5 Editor, the primers generated were designed for Gibson Assembly, and therefore had 20 base-pairs overlap for the flanking DNA. The plasmid backbones were either digested with Thermo Scientific Enzymes for 3 hours at 37°C or amplified via PCR; the backbones were verified by agarose gel electrophoresis and purified by PCR clean up. The insert genes were amplified via PCR and verified by agarose gel electrophoresis. Concentrations of the PCRs were taken at 260 nm and 280 nm on the Nano-Drop 2000 from ThermoScientific. The concentrations and base pairs were used to calculate the volumes of each piece for the Gibson Assembly. The completed Gibson Assembly reaction was transformed into DH5α *E. coli*, using KCM and heat shock to confer permeability of the cell membrane for the plasmid. The transformation reaction was incubated at 37°C with LB broth for 45 minutes to ensure expression of the antibiotic resistance genes. 100 μL of cells were plated on LB and antibiotic agar plates and grown overnight at 37°C. The following day, colonies were screened by Colony PCR with sequencing primers designed for the backbone vector. Colonies with the correct plasmid were lifted off the plate with a pipet tip and mixed into a LB and antibiotic culture. It was grown overnight at 37°C.

For *in vivo* imagining assays, *E. coli* were grown in LB broth and plasmid-appropriate antibiotic unless otherwise noted. Cell cultures were grown overnight in shaker incubator at 37°C.

Each circularly permuted GFP biosensor was designed on pTEV5 for large scale protein expression and purification and designed on pBAD for *in vivo* imaging assays. The dimerization-dependent GFP biosensors were designed on pCDFDUET-1 for *in vivo* imaging assays. The sensors also contain a HIS-tag for protein purification and western blot detection.

in vivo imaging methods

All *E. coli* imaging was completed on the Nikon TiE inverted, epifluorescence microscope. A SpectraX LED system was used for excitation and bandpass emission filters were used to collect emission. All light was collected with an Andor EMCCD camera. FIJI and MicrobeJ were used to analyze microscopy images. In FIJI, the rolling ball method was used for subtracting background. MicrobeJ was used to find cells on phase images and to calculate the average fluorescence in a cell.

The autofluorescence of BL21 cells was imaged. The BL21 cells were grown in LB broth and imaged at OD_{600} 0.5-0.6 on a LB agarose pad.

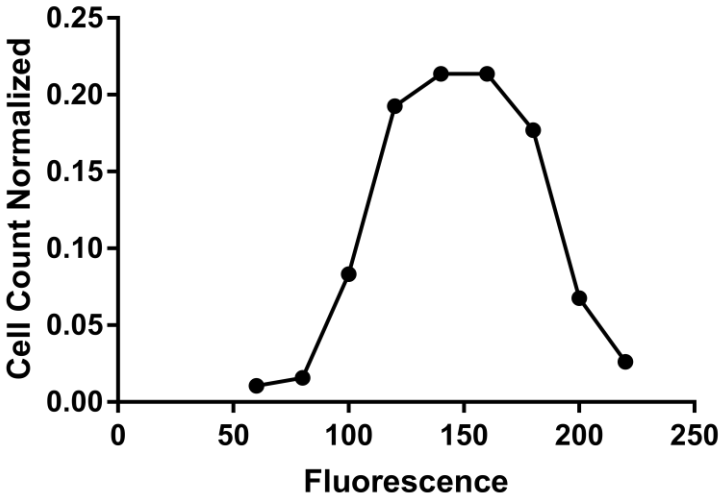

Figure 49: Autofluorescence of BL21 E. coli cells on an LB agarose pad.

cpGFP *in vivo* Wash Assay

Previously, the Laub group has shown washing a strain with fresh media can affect the response of the PhoQP pathway to magnesium. They also proposed 0.01 mM magnesium correlates to the ON state of PhoQP pathway and 10 mM magnesium correlates to the OFF state of PhoQP.[70] I used these methods as the basis for my wash assay design.

Sensor strains were grown overnight in LB broth and AMP. The next morning, the sensors were diluted 1:100 in fresh LB broth and antibiotic, totaling 2 mLs. After reaching critical OD between 0.5-0.6, the cultures were induced with 10 mM arabinose inducer. The cultures were incubated for 2 hours before being collected by centrifugation. The cell pellet was resuspended in M9 broth sans magnesium or and calcium; the resuspension incubated for 5 minutes before collection by centrifugation. This was repeated two times. After the second wash, the cell culture was resuspended and aliquoted into four 0.5 mL amounts. These correspond to the three to four media supplements tested. The aliquots were collected by centrifugation and resuspended in M9 supplemented with 0 mM $MgSO_4$, 0.01 mM $MgSO_4$, 10 mM $MgSO_4$, or 10 mM EDTA (unless otherwise noted). Cells were incubated in the new media for 5 minutes. 1 µL of culture was diluted with 4 µL of DI water before drying on a 1% pure agarose pad of the same supplemented media type from incubation.

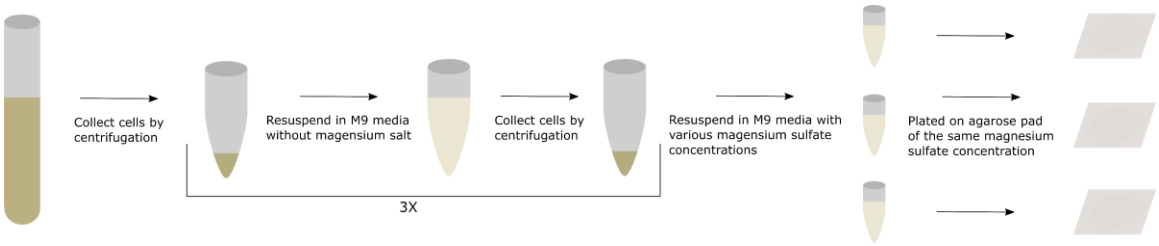

Figure 50: Wash Assay Design: Cells were washed by resuspension in various media before imaging.

Dimerization dependent GFP Biosensor *in vivo* Assay

Sensor strains were grown overnight in M9 broth supplemented with 0 mM $MgSO_4$, 0.01 mM $MgSO_4$, or 10 mM $MgSO_4$, and SPEC. The next morning, the sensors were diluted 1:100 in fresh LB broth and SPEC, totaling 2 mLs. After reaching critical OD between 0.5-0.6, the cultures were induced with 0.5 mM IPTG inducer. The cultures were incubated at 37^o for 2 hours. After, 1 µL of culture was diluted with 4 µL of DI water before drying on a 1% pure agarose pad of the same supplemented media type from incubation.

Protein purification

The sensors were expressed from pBAD expression plasmids that was transformed into chemically competent BL21 (DE3). The cells containing plasmid were plated onto LB-Miller media (50 µg/mL ampicillin plates) and incubated overnight at 37 °C. From a single colony, an overnight 50 mL LB-Miller culture (50 µg/mL ampicillin) was inoculated and incubated overnight at 37 °C. From this saturated culture, 1 L of LB-Miller media (50 µg/mL ampicillin) was inoculated with 10 mL of overnight culture and grown to mid-log phase, OD_{600}= 0.5-0.6. Expression of pBAD plasmid was induced with 10 mM arabinose at 18°C for 16 hours. The cells were

then collected by centrifugation (4˚C, 4000 × *g*, for 30 minutes). The pellet was washed with 20 mL 50 mM HEPES pH 8.0, 500 mM NaCl before being pelleted again by centrifugation (4˚C, 4000 × *g*, for 30 minutes) and stored at -80 °C. Cells were thawed on ice and resuspended in 20 mL of lysis buffer (1 M NaCl, 20 mM Tris-Cl pH 7.4, 20 mM imidazole pH 7.0, 1 mM β-mercaptoethanol [βME], 20 U DNase I, and 0.1% Triton X- 100, supplemented with SIGMAFAST™ protease inhibitor tablets [Sigma]). The cells were lysed by continuous passage through an Avestin EmulsiFlex-C3 at 15,000 psi for 30 minutes. Cell debris was pelleted by centrifugation (4 °C, 20000 × *g*, 30 minutes). The supernatant was then incubated with 1 mL of a 50% slurry of Ni-NTA agarose at 4 °C for 2 hours. The Ni-NTA agarose was separated by centrifugation (700 × *g* for 2 minutes), washed with 3 x 10 mL wash buffer (150 mM NaCl, 20 mM Tris-Cl pH 7.4, 40 mM imidazole pH 7.0, 1 mM βME), and pelleted (700 × *g* for 2 minutes). The Ni-NTA Agarose beads were placed into a gravity column before being eluted with 5- 1 mL portions of elution buffer (150 mM NaCl, 20 mM Tris-Cl pH 7.4, 200 mM imidazole pH 7.0, 1 mM βME). The eluate was concentrated by a 10 kDa MWCO Amicon Centrifugal Filter Unit to 1 mL. The eluate was dialyzed into buffer of 20 mM Tris-Cl and 100 mM NaCL at pH 8.0. 12.5% SDS-page gels were run to confirm expression and subsequent purification of proteins.

Proteins	**Molecular Weight, kDa**	**Extinction Coefficient, $M^{-1}cm^{-1}$**
eGFP	27.764	22,015
$PDC_{C\text{-}term}$ sensor	46.037	62,465
$PDC_{N\text{-}term}$ sensor	46.037	62,340

Figure 51: Table of molecular weights and extinction coefficients of proteins purified

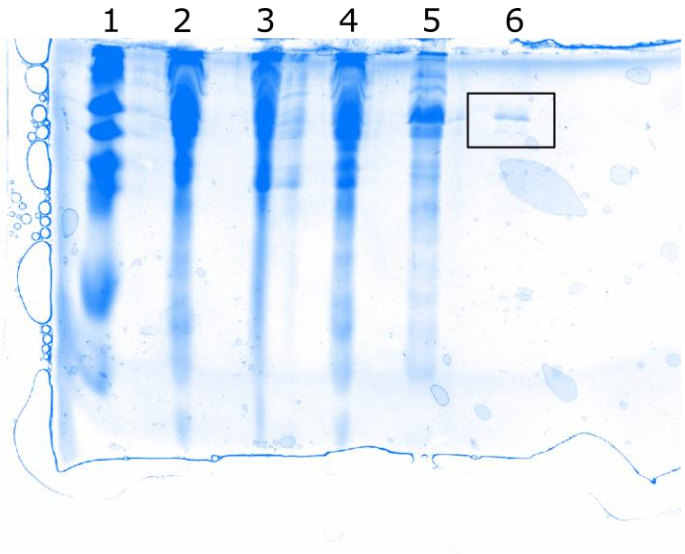

Figure 52: Denaturing SDS gel example: purification of $PDC_{C\text{-}term}$ fusion sensor. Lanes 1: molecular weight ladder; 2: cell pellet after incubation with nickel resin; 3: wash one supernatant; 4: wash two supernatant. 5: wash three supernatant. 6: concentrated elution of protein. The boxed band in lane 6 is at the molecular weight of the sensor.

in vitro fluorescence assay

In a black 96-well plate, protein and magnesium buffer were mixed together following the template laid out below. The covered plate incubated for 10 minutes on ice before fluorescence readings were taken on the Tecan plate reader. The excitation wavelength was 488 nm, and the emission wavelength was 509 nm. The gain was manually set to 116.

	Well	1	2	3	4	5	6
Protein Final Conc. µM- down column		**0.10**	**0.30**	**0.60**	**1.00**	**3.00**	**6.00**
Sterile H_2O- across row	**A**						
0.01 mM $MgSO_4$ final conc- across row	**B**						
0.1 mM $MgSO_4$ final conc- across row	**C**						
1 mM $MgSO_4$ final conc- across row	**D**						
10 mM $MgSO_4$ final conc- across row	**E**						
50 mM $MgSO_4$ final conc- across row	**F**						

Figure 53: Set up of the 96 well plate for the fluorescence assay.

References

1. Juhas, M. E., L. Tümmler, B., Quorum sensing: the power of cooperation in the world of Pseudomonas. *Environmental Microbiology* **2005,** *7*, 459-471.

2. Alford, S. C.; Abdelfattah, A. S.; Ding, Y.; Campbell, R. E., A Fluorogenic Red Fluorescent Protein Heterodimer. *Chemistry and Biology* **2012,** *19 (3)*, 353-360.

3. Bruni, G. N.; Weekley, R. A.; Dodd, B. J. T.; Kralj, J. M., Voltage-gated calcium flux mediates Escherichia coli mechanosensation. *Proceedings of the National Academy of Sciences of the United States of America* **2017,** *114* (35), 9445-9450.

4. Gooderham, W. J.; Hancock, R. E. W., Regulation of virulence and antibiotic resistance by two-component regulatory systems in Pseudomonas aeruginosa. *FEMS Microbiology Reviews* **2009,** *33* (2), 279–294

5. Nadal Jimenez, P. K., G. Thompson, JA. Xavier, KB. Cool, RH. Quax, WJ., The Multiple Signaling Systems Regulating Virulence in Pseudomonas aeruginosa. *Microbiology and Molecular Biology Reviews* **2012,** *76*, 46-65.

6. Fazli, M.; Almblad, H.; Rybtke, M. L.; Givskov, M.; Eberl, L.; Tolker-Nielsen, T., Regulation of biofilm formation in Pseudomonas and Burkholderia species. *Environ Microbiol* **2014,** *16* (7), 1961-81.

7. Lee, J. Z., L., The hierarchy quorum sensing network in Pseudomonas aeruginosa. *Protein & Cell* **2015,** *6*, 26-41.

8. Bains, M.; Fernandez, L.; Hancock, R. E., Phosphate starvation promotes swarming motility and cytotoxicity of Pseudomonas aeruginosa. *Appl Environ Microbiol* **2012,** *78* (18), 6762-8.

9. Zaborin, A.; Romanowski, K.; Gerdes, S.; Holbrook, C.; Lepine, F.; Long, J.; Poroyko, V.; Diggle, S. P.; Wilke, A.; Righetti, K.; Morozova, I.; Babrowski, T.; Liu, D. C.; Zaborina, O.; Alverdy, J. C., Red death in Caenorhabditis elegans caused by Pseudomonas aeruginosa PAO1. *Proceedings of the National Academy of Sciences of the United States of America* **2009,** *106* (15), 6327-32.

10. Lee, J.; Wu, J.; Deng, Y.; Wang, J.; Wang, C.; Wang, J.; Chang, C.; Dong, Y.; Williams, P.; Zhang, L. H., A cell-cell communication signal integrates quorum sensing and stress response. *Nat Chem Biol* **2013,** *9* (5), 339-43.

11. Wu, L.; Estrada, O.; Zaborina, O.; Bains, M.; Shen, L.; Kohler, J. E.; Patel, N.; Musch, M. W.; Chang, E. B.; Fu, Y. X.; Jacobs, M. A.; Nishimura, M. I.; Hancock, R. E.; Turner, J. R.; Alverdy, J. C., Recognition of host immune activation by Pseudomonas aeruginosa. *Science* **2005,** *309* (5735), 774-7.

12. Blier, A. S.; Veron, W.; Bazire, A.; Gerault, E.; Taupin, L.; Vieillard, J.; Rehel, K.; Dufour, A.; Le Derf, F.; Orange, N.; Hulen, C.; Feuilloley, M. G.; Lesouhaitier, O., C-type natriuretic peptide modulates quorum sensing molecule and toxin production in Pseudomonas aeruginosa. *Microbiology* **2011,** *157* (Pt 7), 1929-44.

13. Strempel, N.; Neidig, A.; Nusser, M.; Geffers, R.; Vieillard, J.; Lesouhaitier, O.; Brenner-Weiss, G.; Overhage, J., Human host defense peptide LL-37 stimulates virulence factor production and adaptive resistance in Pseudomonas aeruginosa. *PLoS One* **2013,** *8* (12), e82240.

14. Boursier, M. E.; Moore, J. D.; Heitman, K. M.; Shepardson-Fungairino, S. P.; Combs, J. B.; Koenig, L. C.; Shin, D.; Brown, E. C.; Nagarajan, R.; Blackwell, H. E., Structure-Function Analyses of the N-Butanoyl l-Homoserine Lactone Quorum-

Sensing Signal Define Features Critical to Activity in RhlR. *ACS Chem Biol* **2018,** *13* (9), 2655-2662.

15. Brouwer, S.; Pustelny, C.; Ritter, C.; Klinkert, B.; Narberhaus, F.; Haussler, S., The PqsR and RhlR transcriptional regulators determine the level of Pseudomonas quinolone signal synthesis in Pseudomonas aeruginosa by producing two different pqsABCDE mRNA isoforms. *J Bacteriol* **2014,** *196* (23), 4163-71.

16. Gao, R.; Stock, A. M., Biological insights from structures of two-component proteins. *Annu Rev Microbiol* **2009,** *63*, 133-54.

17. Francis, V. I.; Stevenson, E. C.; Porter, S. L., Two-component systems required for virulence in Pseudomonas aeruginosa. *FEMS Microbiology Letters* **2017,** *364* (11).

18. Mikkelsen, H.; Sivaneson, M.; Filloux, A., Key two-component regulatory systems that control biofilm formation in Pseudomonas aeruginosa. *Environ Microbiol* **2011,** *13* (7), 1666-81.

19. Jimenez, P. N.; Koch, G.; Thompson, J. A.; Xavier, K. B.; Cool, R. H.; Quax, W. J., The multiple signaling systems regulating virulence in Pseudomonas aeruginosa. *Microbiol Mol Biol Rev* **2012,** *76* (1), 46-65.

20. Mulcahy, H.; Charron-Mazenod, L.; Lewenza, S., Extracellular DNA chelates cations and induces antibiotic resistance in Pseudomonas aeruginosa biofilms. *PLoS Pathog* **2008,** *4* (11), e1000213.

21. Lewenza, S., Extracellular DNA-induced antimicrobial peptide resistance mechanisms in Pseudomonas aeruginosa. *Front Microbiol* **2013,** *4*, 21.

22. Gooderham, W. J.; Gellatly, S. L.; Sanschagrin, F.; McPhee, J. B.; Bains, M.; Cosseau, C.; Levesque, R. C.; Hancock, R. E., The sensor kinase PhoQ mediates virulence in Pseudomonas aeruginosa. *Microbiology* **2009,** *155* (Pt 3), 699-711.

23. Groisman, E. A., The Pleiotropic Two-Component Regulatory System PhoP-PhoQ. *Journal of Bacteriology* **2001,** *183* (6), 1835-1842.

24. Cheung, J.; Bingman, C. A.; Reyngold, M.; Hendrickson, W. A.; Waldburger, C. D., Crystal structure of a functional dimer of the PhoQ sensor domain. *J Biol Chem* **2008,** *283* (20), 13762-70.

25. Hendricks, M. R.; Lashua, L. P.; Fischer, D. K.; Flitter, B. A.; Eichinger, K. M.; Durbin, J. E.; Sarkar, S. N.; Coyne, C. B.; Empey, K. M.; Bomberger, J. M., Respiratory syncytial virus infection enhances Pseudomonas aeruginosa biofilm growth through dysregulation of nutritional immunity. *Proceedings of the National Academy of Sciences of the United States of America* **2016,** *113* (6), 1642-7.

26. McRae, R.; Bagchi, P.; Sumalekshmy, S.; Fahrni, C. J., In situ imaging of metals in cells and tissues. *Chem Rev* **2009,** *109* (10), 4780-827.

27. Domaille, D. W.; Que, E. L.; Chang, C. J., Synthetic fluorescent sensors for studying the cell biology of metals. *Nat Chem Biol* **2008,** *4* (3), 168-75.

28. Martynov, V. I.; Pakhomov, A. A.; Popova, N. V.; Deyev, I. E.; Petrenko, A. G., Synthetic Fluorophores for Visualizing Biomolecules in Living Systems. *Acta Naturae* **2016,** *8* (4), 33-46.

29. Noel, S.; Guillon, L.; Schalk, I. J.; Mislin, G. L., Synthesis of fluorescent probes based on the pyochelin siderophore scaffold. *Org Lett* **2011,** *13* (5), 844-7.

30. Palmer, A. E.; Qin, Y.; Park, J. G.; McCombs, J. E., Design and application of genetically encoded biosensors. *Trends Biotechnol* **2011,** *29* (3), 144-52.

31. Lindenburg, L.; Merkx, M., Engineering genetically encoded FRET sensors. *Sensors (Basel)* **2014,** *14* (7), 11691-713.

32. Baird, G. S.; Zacharias, D. A.; Tsien, R. Y., Circular permutation and receptor insertion within green fluorescent proteins. *Proceedings of the National Academy of Sciences of the United States of America* **1999,** *96* (20), 11241-6.

33. Johnsson, N.; Varshavsky, A., Split ubiquitin as a sensor of protein interactions in vivo. *Proceedings of the National Academy of Sciences of the United States of America* **1994,** *91* (22), 10340-4.

34. Park, J. G.; Palmer, A. E., Quantitative measurement of Ca2+ and Zn2+ in mammalian cells using genetically encoded fluorescent biosensors. *Methods Mol Biol* **2014,** *1071*, 29-47.

35. Paige, J. S.; Nguyen-Duc, T.; Song, W.; Jaffrey, S. R., Fluorescence imaging of cellular metabolites with RNA. *Science* **2012,** *335* (6073), 1194.

36. You, M.; Litke, J. L.; Jaffrey, S. R., Imaging metabolite dynamics in living cells using a Spinach-based riboswitch. *Proceedings of the National Academy of Sciences of the United States of America* **2015,** *112* (21), E2756-65.

37. Kellenberger, C. A.; Wilson, S. C.; Sales-Lee, J.; Hammond, M. C., RNA-based fluorescent biosensors for live cell imaging of second messengers cyclic di-GMP and cyclic AMP-GMP. *J Am Chem Soc* **2013,** *135* (13), 4906-9.

38. Kellenberger, C. A.; Wilson, S. C.; Hickey, S. F.; Gonzalez, T. L.; Su, Y.; Hallberg, Z. F.; Brewer, T. F.; Iavarone, A. T.; Carlson, H. K.; Hsieh, Y. F.; Hammond, M. C.,

GEMM-I riboswitches from Geobacter sense the bacterial second messenger cyclic AMP-GMP. *Proceedings of the National Academy of Sciences of the United States of America* **2015,** *112* (17), 5383-8.

39. Fan, J. Y.; Cui, Z. Q.; Wei, H. P.; Zhang, Z. P.; Zhou, Y. F.; Wang, Y. P.; Zhang, X. E., Split mCherry as a new red bimolecular fluorescence complementation system for visualizing protein-protein interactions in living cells. *Biochem Biophys Res Commun* **2008,** *367* (1), 47-53.

40. Robida, A. M.; Kerppola, T. K., Bimolecular fluorescence complementation analysis of inducible protein interactions: effects of factors affecting protein folding on fluorescent protein fragment association. *J Mol Biol* **2009,** *394* (3), 391-409.

41. Hu, C. D.; Chinenov, Y.; Kerppola, T. K., Visualization of interactions among bZIP and Rel family proteins in living cells using bimolecular fluorescence complementation. *Mol Cell* **2002,** *9* (4), 789-98.

42. Filonov, G. S.; Verkhusha, V. V., A near-infrared BiFC reporter for in vivo imaging of protein-protein interactions. *Chem Biol* **2013,** *20* (8), 1078-86.

43. Filonov, G. S.; Piatkevich, K. D.; Ting, L. M.; Zhang, J.; Kim, K.; Verkhusha, V. V., Bright and stable near-infrared fluorescent protein for in vivo imaging. *Nat Biotechnol* **2011,** *29* (8), 757-61.

44. Christen, M.; Kulasekara, H. D.; Christen, B.; Kulasekara, B. R.; Hoffman, L. R.; Miller, S. I., Asymmetrical distribution of the second messenger c-di-GMP upon bacterial cell division. *Science* **2010,** *328* (5983), 1295-7.

45. Komatsu, N.; Aoki, K.; Yamada, M.; Yukinaga, H.; Fujita, Y.; Kamioka, Y.; Matsuda, M., Development of an optimized backbone of FRET biosensors for kinases and GTPases. *Mol Biol Cell* **2011,** *22* (23), 4647-56.

46. Ding, Y.; Li, J.; Enterina, J. R.; Shen, Y.; Zhang, I.; Tewson, P. H.; Mo, G. C.; Zhang, J.; Quinn, A. M.; Hughes, T. E.; Maysinger, D.; Alford, S. C.; Zhang, Y.; Campbell, R. E., Ratiometric biosensors based on dimerization-dependent fluorescent protein exchange. *Nat Methods* **2015,** *12* (3), 195-8.

47. Mehta, S.; Zhang, Y.; Roth, R. H.; Zhang, J. F.; Mo, A.; Tenner, B.; Huganir, R. L.; Zhang, J., Single-fluorophore biosensors for sensitive and multiplexed detection of signalling activities. *Nat Cell Biol* **2018,** *20* (10), 1215-1225.

48. Aper, S. J.; Merkx, M., Rewiring Multidomain Protein Switches: Transforming a Fluorescent Zn(2+) Sensor into a Light-Responsive Zn(2+) Binding Protein. *ACS Synth Biol* **2016,** *5* (7), 698-709.

49. Lee, J.; Natarajan, M.; Nashine, V. C.; Socolich, M.; Vo, T.; Russ, W. P.; Benkovic, S. J.; Ranganathan, R., Surface sites for engineering allosteric control in proteins. *Science* **2008,** *322* (5900), 438-42.

50. Akerboom, J.; Rivera, J. D.; Guilbe, M. M.; Malave, E. C.; Hernandez, H. H.; Tian, L.; Hires, S. A.; Marvin, J. S.; Looger, L. L.; Schreiter, E. R., Crystal structures of the GCaMP calcium sensor reveal the mechanism of fluorescence signal change and aid rational design. *J Biol Chem* **2009,** *284* (10), 6455-64.

51. Berg, J.; Hung, Y. P.; Yellen, G., A genetically encoded fluorescent reporter of ATP:ADP ratio. *Nat Methods* **2009,** *6* (2), 161-6.

52. Honda, Y.; Kirimura, K., Generation of circularly permuted fluorescent-protein-based indicators for in vitro and in vivo detection of citrate. *PLoS One* **2013,** *8* (5), e64597.

53. Belousov, V. V.; Fradkov, A. F.; Lukyanov, K. A.; Staroverov, D. B.; Shakhbazov, K. S.; Terskikh, A. V.; Lukyanov, S., Genetically encoded fluorescent indicator for intracellular hydrogen peroxide. *Nat Methods* **2006,** *3* (4), 281-6.

54. Marvin, J. S.; Schreiter, E. R.; Echevarria, I. M.; Looger, L. L., A genetically encoded, high-signal-to-noise maltose sensor. *Proteins* **2011,** *79* (11), 3025-36.

55. Kitaguchi, T.; Oya, M.; Wada, Y.; Tsuboi, T.; Miyawaki, A., Extracellular calcium influx activates adenylate cyclase 1 and potentiates insulin secretion in MIN6 cells. *Biochem J* **2013,** *450* (2), 365-73.

56. Nausch, L. W.; Ledoux, J.; Bonev, A. D.; Nelson, M. T.; Dostmann, W. R., Differential patterning of cGMP in vascular smooth muscle cells revealed by single GFP-linked biosensors. *Proceedings of the National Academy of Sciences of the United States of America* **2008,** *105* (1), 365-70.

57. Nakai, J.; Ohkura, M.; Imoto, K., A high signal-to-noise Ca(2+) probe composed of a single green fluorescent protein. *Nat Biotechnol* **2001,** *19* (2), 137-41.

58. Wang, Q.; Shui, B.; Kotlikoff, M. I.; Sondermann, H., Structural basis for calcium sensing by GCaMP2. *Structure* **2008,** *16* (12), 1817-27.

59. Nagai, T.; Sawano, A.; Park, E. S.; Miyawaki, A., Circularly permuted green fluorescent proteins engineered to sense Ca2+. *Proceedings of the National Academy of Sciences of the United States of America* **2001,** *98* (6), 3197-202.

60. Kawai, Y.; Sato, M.; Umezawa, Y., Single color fluorescent indicators of protein phosphorylation for multicolor imaging of intracellular signal flow dynamics. *Anal Chem* **2004,** *76* (20), 6144-9.

61. Guntas, G.; Mitchell, S. F.; Ostermeier, M., A molecular switch created by in vitro recombination of nonhomologous genes. *Chem Biol* **2004,** *11* (11), 1483-7.

62. Alicea, I.; Marvin, J. S.; Miklos, A. E.; Ellington, A. D.; Looger, L. L.; Schreiter, E. R., Structure of the Escherichia coli phosphonate binding protein PhnD and rationally optimized phosphonate biosensors. *J Mol Biol* **2011,** *414* (3), 356-69.

63. Marvin, J. S.; Borghuis, B. G.; Tian, L.; Cichon, J.; Harnett, M. T.; Akerboom, J.; Gordus, A.; Renninger, S. L.; Chen, T. W.; Bargmann, C. I.; Orger, M. B.; Schreiter, E. R.; Demb, J. B.; Gan, W. B.; Hires, S. A.; Looger, L. L., An optimized fluorescent probe for visualizing glutamate neurotransmission. *Nat Methods* **2013,** *10* (2), 162-70.

64. Cheung, J.; Hendrickson, W. A., Sensor domains of two-component regulatory systems. *Curr Opin Microbiol* **2010,** *13* (2), 116-23.

65. Wang, S., Bacterial two-component systems: structures and signaling mechanisms. In *Protein Phosphorylation in Human Health* [Online] InTech: 2012.

66. Molnar, K. S.; Bonomi, M.; Pellarin, R.; Clinthorne, G. D.; Gonzalez, G.; Goldberg, S. D.; Goulian, M.; Sali, A.; DeGrado, W. F., Cys-scanning disulfide crosslinking and bayesian modeling probe the transmembrane signaling mechanism of the histidine kinase, PhoQ. *Structure* **2014,** *22* (9), 1239-1251.

67. Cheung, J.; Hendrickson, W. A., Crystal structures of C4-dicarboxylate ligand complexes with sensor domains of histidine kinases DcuS and DctB. *J Biol Chem* **2008,** *283* (44), 30256-65.

68. Affandi, T.; Issaian, A. V.; McEvoy, M. M., The Structure of the Periplasmic Sensor Domain of the Histidine Kinase CusS Shows Unusual Metal Ion Coordination at the Dimeric Interface. *Biochemistry* **2016,** *55* (37), 5296-306.

69. Nadler, D. C.; Morgan, S. A.; Flamholz, A.; Kortright, K. E.; Savage, D. F., Rapid construction of metabolite biosensors using domain-insertion profiling. *Nat Commun* **2016,** *7*, 12266.

70. Salazar, M. E.; Podgornaia, A. I.; Laub, M. T., The small membrane protein MgrB regulates PhoQ bifunctionality to control PhoP target gene expression dynamics. *Mol Microbiol* **2016,** *102* (3), 430-445.

71. Regelmann, A. G.; Lesley, J. A.; Mott, C.; Stokes, L.; Waldburger, C. D., Mutational analysis of the Escherichia coli PhoQ sensor kinase: differences with the Salmonella enterica serovar Typhimurium PhoQ protein and in the mechanism of Mg2+ and Ca2+ sensing. *J Bacteriol* **2002,** *184* (19), 5468-78.

72. Miyashiro, T.; Goulian, M., Stimulus-dependent differential regulation in the Escherichia coli PhoQ PhoP system. *Proceedings of the National Academy of Sciences of the United States of America* **2007,** *104* (41), 16305-10.

73. Brunia, G. N.; Weekley, R. A.; Dodd, B. J.; Kralj, J. M., Voltage-gated calcium flux mediates *Escherichia coli* mechanosensation. *PNAS* **2017,** *114* (35), 9445-9450.

74. Chen, T. W.; Wardill, T. J.; Sun, Y.; Pulver, S. R.; Renninger, S. L.; Baohan, A.; Schreiter, E. R.; Kerr, R. A.; Orger, M. B.; Jayaraman, V.; Looger, L. L.; Svoboda, K.; Kim, D. S., Ultrasensitive fluorescent proteins for imaging neuronal activity. *Nature* **2013,** *499* (7458), 295-300.

75. Thomas, J. D.; Daniel, R. A.; Errington, J.; Robinson, C., Export of active green fluorescent protein to the periplasm by the twin-arginine translocase (Tat) pathway in Escherichia coli. *Mol Microbiol* **2001,** *39* (1), 47-53.

76. Alford, S. C.; Ding, Y.; Simmen, T.; Campbell, R. E., Dimerization-dependent green and yellow fluorescent proteins. *ACS Synth Biol* **2012,** *1* (12), 569-75.

77. Shaner, N. C.; Campbell, R. E.; Steinbach, P. A.; Giepmans, B. N.; Palmer, A. E.; Tsien, R. Y., Improved monomeric red, orange and yellow fluorescent proteins derived from Discosoma sp. red fluorescent protein. *Nat Biotechnol* **2004,** *22* (12), 1567-72.

78. Terskikh, A. V.; Fradkov, A. F.; Zaraisky, A. G.; Kajava, A. V.; Angres, B., Analysis of DsRed Mutants. Space around the fluorophore accelerates fluorescence development. *J Biol Chem* **2002,** *277* (10), 7633-6.

79. Ai, H. W.; Henderson, J. N.; Remington, S. J.; Campbell, R. E., Directed evolution of a monomeric, bright and photostable version of Clavularia cyan fluorescent protein: structural characterization and applications in fluorescence imaging. *Biochem J* **2006,** *400* (3), 531-40.

80. West, A. H.; Stock, A. M., Histidine kinases and response regulator proteins in two-component signaling systems. *Trends Biochem Sci* **2001,** *26* (6), 369-76.

81. Gao, R.; Tao, Y.; Stock, A. M., System-level mapping of Escherichia coli response regulator dimerization with FRET hybrids. *Mol Microbiol* **2008,** *69* (6), 1358-72.